

DIFFERENTIAL POLARIZATION IMAGING

I. Theory

MYEONGHEE KIM, DAVID KELLER, AND CARLOS BUSTAMANTE

Department of Chemistry, The University of New Mexico, Albuquerque, New Mexico 87131

ABSTRACT A theory of differential polarization imaging is derived using Mueller calculus. It is shown that, for any arbitrary object, 16 images (in general different) can be obtained by combining different incident polarizations of light and measuring the specific polarization components transmitted or scattered by the object. These are called the Mueller images of the object. Mathematical expressions of these images for an object of arbitrary geometry are derived using classical vector diffraction theory and the paraxial and thin lens approximations. The object is described as a collection of point polarizable groups. The electromagnetic fields are calculated using the first Born-Approximation, but extension of the theory to higher-order approximations is shown to be straightforward. These expressions are obtained for the transmission, or bright-field, geometry, and the scattering, or dark-field, configuration. In both cases, the contributions of scattering, absorption, and background illumination to the Mueller images are characterized. The contributions of linear dichroism, circular dichroism, and linear and circular intensity differential scattering to certain Mueller images are established. It is shown that the Mueller images represent a complete two-dimensional mapping of the molecular anisotropy of the object.

I. INTRODUCTION

Differential polarization imaging is a method in which the images of an object, obtained using light of orthogonal incident polarizations, are subtracted point by point from each other. The resulting difference image will display both magnitude and sign whose values will vary according to location in the image. In order for the difference between these images not to vanish, the objects must be optically anisotropic and therefore able to interact preferentially with one polarization over the other. Conversely, the differential polarization images of optically isotropic objects vanish identically because these objects cannot discriminate between different polarizations of the incident light. Thus, the differential polarization image represents a two-dimensional map of the optical anisotropy of the object which, in this technique, provides a contrast mechanism between an object and its surroundings. When the object is structurally inhomogeneous, this contrast mechanism permits the spatial resolution of adjacent domains of different optical anisotropy within the object.

Applications of this technique to microscopy are of particular interest as this method provides a way of probing directly the molecular organization of the specimen studied. The microscopic specimen can be whole cells in a particular metabolic state or in a given phase of their life cycle, i.e., isolated macromolecular aggregates, such as chromosomes, membrane systems, tissues, etc. However, application of this method is by no means restricted to biological systems, and the studied specimen can be opti-

cally thin liquid crystal samples, polymeric surface coatings, or polymer organizations in the presence or absence of external fields, etc. Furthermore, nontransparent optically anisotropic samples can be studied in reflection to combine the power of surface ellipsometry methods with the imaging capabilities into what can be called imaging or spaced-resolved ellipsometry.

The information obtained by this new method is not restricted to static structural features in the specimen. By measuring the fluorescence polarization emitted by a selectively labeled specimen, it is possible to carry out space-resolved (imaging) fluorescence depolarization studies in which the dynamical information is displayed as a function of position in the image.

Recently, the first prototypes of differential polarization microscopes have been built (1, 2) and the first differential polarization images have been obtained (3–5). These results have confirmed the potential of this imaging technique in its specificity to select and resolve microscopic domains of distinct optical anisotropy in the object.

It is important to establish this method on solid theoretical ground for it combines the principles of polarization spectroscopy with the physics of image formation. With the exception of the simplest of polarization combinations, a priori interpretations of the resulting images can be difficult. Furthermore, such theoretical treatment must establish the number and nature of the independent polarization combinations required to exhaust the information obtainable from these imaging experiments. Lastly, the theory must guide the experimentalist in the choice of the

polarization combinations appropriate to the object under study.

The first theory of differential polarization imaging, restricted to the case of incident circular polarizations, has recently appeared (6). In this paper, we present a generalization of this theory to include all possible combinations of incident polarizations and their modification after interacting with the object. In describing this interaction, we have considered only linear optical effects corresponding to the usual refractive and absorptive phenomena.

In deriving this theory, a number of approximations have been used. These are clearly pointed out throughout the derivation along with the limitations on applicability that they impose on the theory.

II. THE MUELLER FORMULATION

A. The Stokes Parameters

In developing a theory of differential polarization imaging, we must describe the interaction of objects with light of any given polarization. We adopt the Mueller formulation which uses four parameters to describe the intensity and the state of polarization of the light. These are called the Stokes parameters (7)

$$\begin{aligned}\mathcal{I} &= I^H + I^V & (1) \\ \mathcal{Q} &= I^H - I^V \\ \mathcal{U} &= I^{+45^\circ} - I^{-45^\circ} \\ \mathcal{V} &= I^R - I^L,\end{aligned}$$

where I^H represents the intensity of the horizontal component of the light relative to a reference plane and I^V represents the intensity of the vertical component of the light. Similarly, I^{+45° , I^{-45° , I^R , and I^L describe the intensities of $+45^\circ$ linearly polarized, -45° linearly polarized, right circular, and left circular components of the light, respectively. Therefore the first Stokes parameter, \mathcal{I} , describes the total intensity of the light and \mathcal{Q} represents, depending on its sign, the horizontal or vertical polarization preference of the light. \mathcal{U} represents the $+45^\circ$ or -45° polarization preference of the light, and \mathcal{V} represents the right- or left-circular polarization preference of light. These four parameters can be arranged to form a 4×1 column matrix, which is called the Stokes Vector (7). If the light is totally polarized, i.e., if there is no statistical randomness in the polarization, conservation of energy arguments (8) show that

$$\mathcal{I}^2 = \mathcal{Q}^2 + \mathcal{U}^2 + \mathcal{V}^2.$$

In this description unpolarized light is represented by the vector (1, 0, 0, 0) (the elements of the Stokes vector are usually normalized by dividing them by \mathcal{I}). Horizontally polarized light, (1, 1, 0, 0); vertically, (1, -1, 0, 0); $+45^\circ$ linear polarization, (1, 0, 1, 0); -45° , (1, 0, -1, 0); right-circularly polarized light, (1, 0, 0, 1); and left, (1, 0, 0, -1).

When light of a well-defined incident polarization interacts with an object, the state of polarization of the light transmitted or scattered by the object will be modified according to the optical anisotropy of the object (which in turn depends on its structure) and the nature of the incident polarization of the light. The intensity and polarization of the transmitted or scattered light are linearly related to those of the incident light according to

$$\mathbf{S} = \mathbf{M}\mathbf{S}_0,$$

where \mathbf{S}_0 is the Stokes vector, which describes the polarization state of the incident light, and \mathbf{S} is the Stokes vector representing the polarization state of the light scattered or transmitted by an object. The ability of the object to modify the polarization of the incident light is described by the transformation matrix \mathbf{M} , called the Mueller matrix of the object. This matrix is specific to each object and depends on the structure of the object. Its sixteen entries represent the most complete characterization of the optical anisotropy of the object. They are a function of the wavelength of light and the scattering angle. Experimentally these entries can be measured by using light of different states of polarization to probe the object and by measuring different polarization components of the light transmitted or scattered by the object. Thus we can write the Mueller matrix elements as sums and differences of intensities that are experimentally measurable.

Table I shows the sixteen entries of the Mueller matrix written in terms of measurable intensities. Here the subscripts indicate the polarization state of the incident light and the superscripts indicate the intensity of a polarization component of the light as measured by placing the appropriate analyzer before the detector. No subscript means that the incident light is unpolarized and no superscript indicates that the total intensity of the light reaching the detector is measured and that no particular polarization component is selected by means of an analyzer. A similar table, although with somewhat different nomenclature, has been presented by Bickel (9). From Table I we see that the relevant information about the object contained in the elements of the Mueller matrix can only be accessed by differences between intensities. This is why differential polarization methods are more sensitive than regular spectroscopic methods to the structural details of an object.

B. The Mueller Images

Let us now imagine that an imaging device, such as a lens, is placed between the object and a detector screen and is used to generate an image of the object. Furthermore, if at each point on this image the intensities are processed according to Table I, 16 differential polarization images of the object can be generated. We call these images the Mueller images of the object. Different elements of the Mueller matrix of a molecule carry information on complementary symmetry aspects of the molecule, so these images

TABLE I
THE SIXTEEN ENTRIES OF MUELLER MATRIX EXPRESSED IN TERMS OF THE MEASURABLE INTENSITIES

$M_{11} = \frac{I}{I}$	$M_{12} = \frac{I_H - I_V}{I_H + I_V}$	$M_{13} = \frac{I_{+45} - I_{-45}}{I_{+45} + I_{-45}}$	$M_{14} = \frac{I_R - I_L}{I_R + I_L}$
$M_{21} = \frac{I^H - I^V}{I^H + I^V}$	$M_{22} = \frac{I_H^H - I_H^V - (I_V^H - I_V^V)}{I_H^H + I_H^V + I_V^H + I_V^V}$	$M_{23} = \frac{I_{+45}^H - I_{+45}^V - (I_{-45}^H - I_{-45}^V)}{I_{+45}^H + I_{+45}^V + I_{-45}^H + I_{-45}^V}$	$M_{24} = \frac{I_R^H - I_R^V - (I_L^H - I_L^V)}{I_R^H + I_R^V + I_L^H + I_L^V}$
$M_{31} = \frac{I^{+45} - I^{-45}}{I^{+45} + I^{-45}}$	$M_{32} = \frac{I_H^{+45} - I_H^{-45} - (I_V^{+45} - I_V^{-45})}{I_H^{+45} + I_H^{-45} + I_V^{+45} + I_V^{-45}}$	$M_{33} = \frac{I_{+45}^{+45} - I_{+45}^{-45} - (I_{-45}^{+45} - I_{-45}^{-45})}{I_{+45}^{+45} + I_{+45}^{-45} + I_{-45}^{+45} + I_{-45}^{-45}}$	$M_{34} = \frac{I_R^{+45} - I_R^{-45} - (I_L^{+45} - I_L^{-45})}{I_R^{+45} + I_R^{-45} + I_L^{+45} + I_L^{-45}}$
$M_{41} = \frac{I^R - I^L}{I^R + I^L}$	$M_{42} = \frac{I_H^R - I_H^L - (I_V^R - I_V^L)}{I_H^R + I_H^L + I_V^R + I_V^L}$	$M_{43} = \frac{I_{+45}^R - I_{+45}^L - (I_{-45}^R - I_{-45}^L)}{I_{+45}^R + I_{+45}^L + I_{-45}^R + I_{-45}^L}$	$M_{44} = \frac{I_R^R - I_R^L - (I_L^R - I_L^L)}{I_R^R + I_R^L + I_L^R + I_L^L}$

can be seen as two-dimensional maps of the optical anisotropy of the imaged object. Furthermore, different domains of the object will have Mueller matrix elements of different values associated with them. In this way adjacent domains in the object, which differ in their optical anisotropy, can be distinguished and spatially resolved. On the contrary, totally isotropic domains in the object will interact identically with light of different polarization. In these regions the differences indicated in Table I vanish. As a result the differential imaging technique will provide a polarization-dependent contrast between an object and its background, and between different domains in the object.

There are two mechanisms that can contribute to the generation of the Mueller images. The first process is due to differential absorption and refraction of the orthogonal polarizations by the object. When plane polarized light is used, the differential image obtained will then be a bi-dimensional map of the linear dichroism and linear birefringence of the object. This corresponds to the Mueller image M_{12} , as will be shown later. With circularly polarized light the differential image maps the circular dichroism and circular birefringence of the specimen (the M_{14} element of the Mueller matrix) and so on. A second mechanism is due to the preferential scattering of the

orthogonal polarization pair by the object. This mechanism will contribute to the differential polarization image both inside and outside the absorption band. For wavelengths outside the absorption bands of the object, the M_{12} image maps the linear intensity differential scattering (LIDS) of the object, and M_{14} is related to the CIDS, or circular intensity differential scattering.

The optical train can be arranged in two different imaging geometries. In the first one, called dark-field imaging (see Fig. 1), the light scattered by the object at a given angle is captured by the lens to form the image. In this case the lens and the detector screen are placed at an angle to the incident beam. Here the image appears as bright intensities on an otherwise dark background. The second geometry corresponds to bright-field imaging (see Fig. 1), in which the light transmitted by the object is used to generate the image. Here the lens and the screen are placed directly behind the sample. The image appears in this case as a dark region (shadow) in an otherwise bright background. The mechanisms mentioned above, i.e., preferential absorption, refraction, and scattering of polarized light, can contribute to the dark- and bright-field differential polarization images. However, the absorption mechanism, when present, is the dominant effect on bright-field

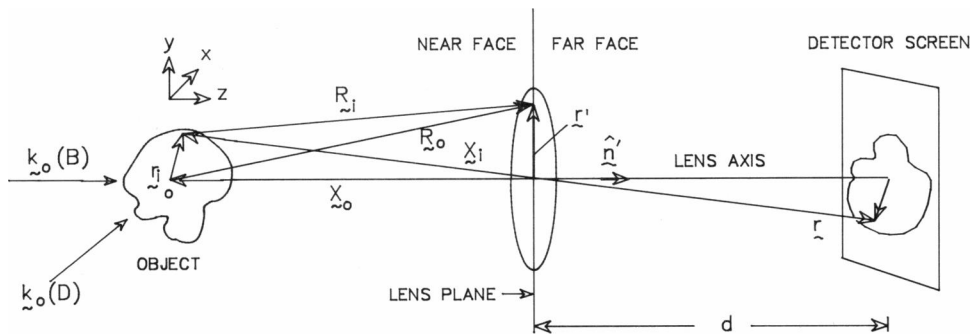


FIGURE 1 Geometry for the calculation of the Mueller matrix images. The wave vectors \mathbf{k}_o show the direction of the light which illuminates the object for the bright-field imaging (B) and for the dark-field imaging (D). \mathbf{r}_i is the position vector of the i th polarizable group inside the object and \mathbf{r}' is the position vector on the lens plane. The other variables are: \mathbf{R}_0 is the vector that points from the origin of the object to the arbitrary point on the lens plane and $\mathbf{R}_i = \mathbf{R}_0 - \mathbf{r}_i$. The vector \mathbf{x}_0 points from the center of the lens to the origin of the object $\mathbf{x}_i = \mathbf{x}_0 + \mathbf{r}_i$. \mathbf{n}' is the unit vector that is normal to the surface of the lens and \mathbf{r} points from the center of the lens to a image point on the detector screen. d is the distance between the lens and the detector screen. The face of the lens that is toward the object is called the near face of the lens and the opposite face of the lens is called the far face of the lens.

imaging, while the scattering mechanism dominates dark-field imaging.

So far our approach has been phenomenological. The next step is to obtain the expressions for the sixteen elements of the Mueller images from classical electrodynamics and vector diffraction theory. This task will be accomplished in the following section.

III. THEORY OF MUELLER IMAGING

The magnitude and sign adopted by the entries of the Mueller matrix at every point on the image plane constitute the sixteen Mueller images of the object. In this section we will derive the explicit expressions for the Mueller image entries of Table I. This will be done for an arbitrary geometry of the object and for any incident and measured polarization component of the light. For simplicity the imaging element will be a single thin lens.

A. Scheme of the Derivation

When light impinges upon a molecule, the electric field of the electromagnetic radiation produces a distortion of its charge density. Such distortion can be described in a first approximation as the induction of oscillating electric dipole moments. The direction and magnitude of the induced dipole depend both on the direction of the incident field and the polarizability tensor of the molecule. In turn, these oscillating dipole moments give rise to scattering and absorption of the electromagnetic radiation, the two main mechanisms contributing to the optical image of an object. Accordingly, the explicit expressions for the Mueller images will be derived following these steps: (a) An object is described by a collection of point polarizable groups with a polarizability tensor defined at each group. (b) The light arriving at the lens is obtained using classical scattering theory in the first Born-Approximation. (c) The lens, assumed to be thin, operates on the fields arriving at its near face. Only rays traveling parallel or almost parallel to the lens axis are described exactly by the theory (paraxial approximation). (d) The light intensity arriving at the detector (image plane) is obtained using classical vector diffraction theory.

As described briefly above, we are treating the simple image formation by a single thin lens. Our purpose in developing this theory is to obtain an understanding of the properties of the differential polarization images and not to simulate any instrumental optical train.

B. Dark-Field Equations

1. The Electric Field on the Near Face of the Lens. In dark-field imaging, only the light scattered by the object arrives at the near face of the lens. In this section we will obtain the form of the electric field scattered by the object for an arbitrary incident polarization.

The electric field, due to a collection of the oscillating dipole moments, induced inside an object by the incident

light is written (10)

$$\mathbf{E}_{\text{ind}}(\mathbf{r}') = 4\pi k^2 \int \Gamma(\mathbf{r}' - \mathbf{x}) \cdot \alpha(\mathbf{x}) \cdot \mathbf{E}(\mathbf{x}) d^3x, \quad (2)$$

where the subscript "ind" stands for "induced," $k = 2\pi/\lambda$ is the wave number of the incident light, $\alpha(\mathbf{x})$ is the polarizability density at position \mathbf{x} in the object, $\mathbf{E}(\mathbf{x})$ is the electric field at \mathbf{x} , and $\Gamma(\mathbf{r}' - \mathbf{x})$ is a tensor Green's function that gives the electric field at \mathbf{r}' caused by a collection of induced dipoles $\mu(\mathbf{x}) = \alpha(\mathbf{x}) \cdot \mathbf{E}(\mathbf{x})$, at position \mathbf{x} . The volume integral extends over the entire volume occupied by the object. If the object is composed of discrete polarizable groups, the integral sign is replaced by a summation sign and Eq. 2 is rewritten as

$$\mathbf{E}_{\text{ind}}(\mathbf{r}') = 4\pi k^2 \sum_i \Gamma(\mathbf{r}' - \mathbf{x}_i) \cdot \alpha_i \cdot \mathbf{E}(\mathbf{x}_i), \quad (3)$$

where α_i is the polarizability tensor of the i th polarizable group and $\mathbf{E}(\mathbf{x}_i)$ is the electric field experienced by the i th polarizable group. In our derivation, we use the first Born-Approximation in which $\mathbf{E}(\mathbf{x}_i)$ is replaced by the incident electric field $\mathbf{E}_0(\mathbf{x}_i)$, and the interactions between induced dipole moments inside the sample are neglected. The effects of dipole-dipole interactions can be taken into account by the use of higher order Born-Approximations as will be shown later. The Green's function Γ has three contributions: (a) static dipole field, (b) intermediate field, and (c) radiation field. The scattered electric field on the near face of the lens can be obtained from Eq. 3 by taking only the radiation term in Γ . In this approximation, $\Gamma(\mathbf{r}' - \mathbf{x}_i) = \Gamma(\mathbf{R}_i)$ becomes

$$\Gamma(\mathbf{R}_i) = \frac{e^{ikR_i}}{4\pi R_i} (\mathbf{I} - \hat{\mathbf{R}}_i \hat{\mathbf{R}}_i),$$

where \mathbf{R}_i is the distance vector from the i th group in the object to position \mathbf{r}' on the surface of the lens, measured from its center (see Fig. 1), and R_i is the magnitude of \mathbf{R}_i . This approximation is reasonable because the distance between the object and the lens is much larger than the wavelength of the light (11). The electric field on the near face of the lens for dark-field imaging can then be written (11)

$$\mathbf{E}_{\text{scat}}(\mathbf{r}') \approx k^2 \sum_i \frac{e^{ikR_i}}{R_i} (\mathbf{I} - \hat{\mathbf{R}}_i \hat{\mathbf{R}}_i) \cdot \alpha_i \cdot \mathbf{E}_0(\mathbf{x}_i), \quad (4)$$

where $\hat{\mathbf{R}}_i$ is the unit vector of \mathbf{R}_i (refer to Fig. 1) and \mathbf{i} is the unit tensor. By analogy, $\alpha_i \cdot \mathbf{E}_0(\mathbf{x}_i)$ is the i th oscillating electric dipole moment generated at \mathbf{x}_i by the incident electric field $\mathbf{E}_0(\mathbf{x}_i)$. The factor e^{ikR_i}/R_i appearing in Eq. 4 shows that the scattered electric field is a spherical wave propagating away from the object. The tensor $(\mathbf{I} - \hat{\mathbf{R}}_i \hat{\mathbf{R}}_i)$ ensures the transversality of this wave.

In the above equations, the response of a group to the incident light is described by the polarizability tensor, α_i . In this description, each polarizable group may contain a

very large number of atoms or molecules, but the groups are assumed to be small compared with the wavelength inside the object. The latter condition is necessary if only dipole contributions are to be considered.

If the groups are optically active, their internal asymmetry is manifest in their response to incident light. In this case, the induced dipole moment, μ , is given by (12)

$$\mu = \alpha \cdot \mathbf{E} + \frac{\beta \partial \mathbf{B}}{c \partial t},$$

where c is the speed of light in a vacuum, \mathbf{B} is the magnetic field strength, and β is a parameter proportional to the rotational strength of the group. In the first Born-Approximation, \mathbf{E} in the above equation is an incident plane wave and this equation may be rewritten

$$\mu_j = \sum_l (\alpha_{jl} - i\beta \epsilon_{jkl} k_k) E_l,$$

where μ_j is the j th cartesian component of μ , ϵ_{jkl} is the Levi-Civita tensor, and k_k and E_l are the k th and the l th cartesian components of the wave vector \mathbf{k} and \mathbf{E} , respectively. The quantity inside the parentheses of the above equation can be thought of as a tensor that plays the role of the polarizability tensor for optically active groups. The polarizability tensor α is symmetric, i.e., $\alpha_{jl} = \alpha_{lj}$. However, notice that $\epsilon_{jkl} k_k$ is an antisymmetric tensor and depends on the direction of propagation of the incident light. This optical activity not explicitly derived in the theory is referred to as ‘‘intrinsic optical activity.’’ In bright-field imaging, this is the only optical activity effect that can be described when a first Born-Approximation is used. For those arising from the coupling between groups bearing a chiral arrangement with respect to each other require higher Born-Approximations, as will be seen later. In the dark-field imaging, on the other hand, preferential scattering of the circular polarizations can contribute to the optical activity of the image in the first Born-Approximation.

2. The Effect of the Lens on the Electric Field. When light enters a lens, its direction, phase, and polarization are changed. In general this modification will depend on the refractive index of the lens, its radius of curvature, the angle of incidence, and the state of polarization of the light. A detailed description of all these effects can become very cumbersome and therefore here we will assume that the lens affects the electric field only in the following two ways: (a) The phase of the electric field is modified as a function of position in the lens plane. We use a single thin lens as imaging device and this implies that a ray entering at coordinates (r') on one face of the lens (see Fig. 1) emerges at the same coordinates on the opposite face. Therefore, a thin lens can be considered as a simple phase transformer. (b) A modification of the polarization of the electric field to maintain the transversality of the

fields. That is, when the direction of propagation of the electric field is changed by the lens, the polarization changes accordingly.

The phase modification introduced by the lens on the fields is given by $e^{i\phi(r')}$, where r' is the magnitude of \mathbf{r}' and $\phi(r')$ is the total phase delay experienced by the wave at coordinates \mathbf{r}' in passing through the lens. This delay is given by (13)

$$\phi(r') = kn\Delta(r') + k[\Delta_0 - \Delta(r')], \quad (5)$$

where n is the refractive index of the lens material, Δ_0 is the thickness of the lens at its center, and $\Delta(r')$, the thickness function, is the thickness of the lens at position \mathbf{r}' . The first term $kn\Delta(r')$ is the phase delay caused by the lens, and the second term $k[\Delta_0 - \Delta(r')]$ is the phase delay caused by the free region between the two planes P_1 and P_2 in Fig. 2. Rearranging Eq. 5, we obtain

$$\phi(r') = k\Delta_0 + k(n-1)\Delta(r'). \quad (6)$$

The thickness function $\Delta(r')$ is given by (13)

$$\Delta(r') = \Delta_0 - \frac{r'}{2} \left(\frac{1}{R_1} - \frac{1}{R_2} \right), \quad (7)$$

where R_1 and R_2 are the radii of curvature of the lens surfaces. Eq. 7 is only valid in the paraxial approximation (14). That is, we consider only portions of the wavefront that lie near the lens axis ($r' \ll R_1$ and $r' \ll R_2$). Substituting Eq. 7 and the lens maker's formula,

$$\frac{1}{f} = (n-1) \left(\frac{1}{R_1} - \frac{1}{R_2} \right)$$

into Eq. 6, we obtain

$$\phi(r') = kn\Delta_0 - \frac{k(r')^2}{2f}. \quad (8)$$

The phase modification introduced by the lens on the waves arriving at its near face can be written as

$$\exp \left[i \left(kn\Delta_0 - \frac{k(r')^2}{2f} \right) \right].$$

To derive the function that gives the effect of the lens on the incident polarization, we first make the far-field approximation to the scattered electric field. That is, we

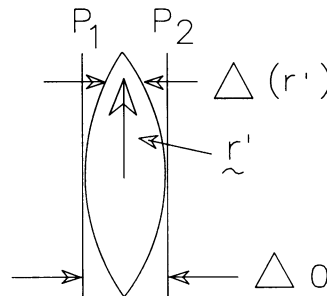


FIGURE 2 The thickness function $\Delta(r')$.

take $\hat{\mathbf{R}}_i$ in Eq. 4 to be approximately $\hat{\mathbf{R}}_0$, which is the unit vector along \mathbf{R}_0 pointing from the origin of the sample to \mathbf{r}' (see Figs. 1 and 3). Also R_i is taken to be approximately equal to $R_0 - \mathbf{R}_0 \cdot \mathbf{r}_i$, where $R_0 = |\mathbf{R}_0|$. These approximations are reasonable because the dimensions of the sample are much smaller than the distance between the sample and the lens ($r_i \ll r_0$, where $r_i = |\mathbf{r}_i|$ and r_0 is the magnitude of \mathbf{x}_0 which points from the origin of the lens to the origin of the sample). Eq. 4 then becomes

$$\mathbf{E}_{\text{scatt}}(\mathbf{r}') \approx \frac{k^2 e^{ikR_0}}{R_0} (\mathbf{1} - \hat{\mathbf{R}}_0 \hat{\mathbf{R}}_0) \cdot \sum_i e^{-ik\hat{\mathbf{R}}_0 \cdot \mathbf{r}_i} \alpha_i \cdot E_0 e^{i\mathbf{k}_0 \cdot \mathbf{x}_i} \hat{\mathbf{e}}_0, \quad (9)$$

where E_0 is the amplitude of the incident electric field of the light, and \mathbf{k}_0 and $\hat{\mathbf{e}}_0$ are the wave vector and the polarization unit vector of the incident light, respectively. The scattered electric field on the near face of the lens, shown in Eq. 9, has the form of a spherical wave centered on the point \mathbf{x}_0 . If the lens is a perfect lens that works according to the Gaussian lens formula, $1/r_0 + 1/d - 1/f = 0$ (15), where d is the distance between the lens and the imaging plane, and f is the focal length of the lens, then the electric field on the far side of the lens will have the form of a spherical wave centered on the point $-\mathbf{m}\mathbf{x}_0$ (m being the magnification of the lens) (see Fig. 3).

The unit vector that points toward the point $-\mathbf{m}\mathbf{x}_0$ from \mathbf{r}' is $-(\mathbf{r}' + \mathbf{m}\mathbf{x}_0)/|\mathbf{r}' + \mathbf{m}\mathbf{x}_0|$, and the tensor that ensures that the electric field on the far side of the lens is transversal is

$$\mathbf{P}(\mathbf{r}') = P \left[\mathbf{1} - \frac{(\mathbf{r}' + \mathbf{m}\mathbf{x}_0)(\mathbf{r}' + \mathbf{m}\mathbf{x}_0)}{|\mathbf{r}' + \mathbf{m}\mathbf{x}_0|^2} \right], \quad (10)$$

where P is a constant that depends on the transmittance of the lens material and on \mathbf{r}' .

Eq. 10 assumes that no substantial depolarization of the light occurs as it travels from air into the refractive medium of the lens. This approximation is valid only for normal or near-normal incidence on the lens surface, i.e., in the paraxial approximation. In the general case, when the light reaches the refractive interface, selective refraction and transmission of the orthogonal components of the polarization vector will occur. The modification of the polarization of the light induced by these effects is larger when the angle of incidence is more oblique and increases with the difference between the refractive indices of the

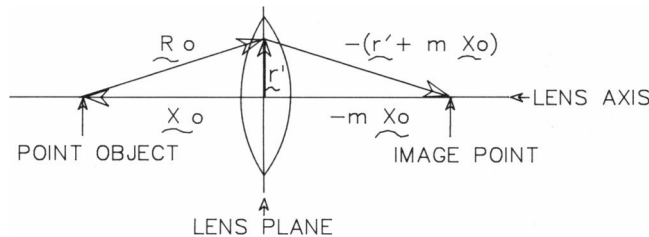


FIGURE 3 Geometry for the derivation of the tensor $\mathbf{P}(\mathbf{r}')$.

two media. The description of these effects requires the use of the Fresnel equations (14, 15) and will be neglected here because of the paraxial assumption.

The electric field on the far face of the lens, before it propagates outward from the lens, is written

$$\mathbf{E}_{\text{far}}(\mathbf{r}') = \mathbf{P}(\mathbf{r}') e^{ik(r')} \mathbf{E}_{\text{near}}(\mathbf{r}'), \quad (11)$$

where the subscript "far" labels the far face of the lens and the \mathbf{E}_{near} indicates the field arriving at the near face of the lens. Eq. 11 is valid for bright-field as well as dark-field geometries. In the case of the dark-field experiment, $\mathbf{E}_{\text{near}}(\mathbf{r}')$ in Eq. 11 coincides with $\mathbf{E}_{\text{scatt}}(\mathbf{r}')$ given by Eq. 9.

3. Image Field on the Detector Screen. Once we know the electric field on the far face of the lens, we treat the propagation of the waves by using vector diffraction theory in the Fresnel limit to obtain the polarization dependent image on the detector screen. The Fresnel limit must be used when the dimensions of the diffracting aperture (in our case the radius of the lens, are much larger than the wavelength of the light) (11). This limit must be used even though the size of the aperture is much smaller than the distance to the imaging plane, i.e., $a/d \ll 1$, since

$$\frac{k_0 a^2}{d} \approx 1,$$

where $k_0 = 2\pi/\lambda$ as before.

In this limit, the electric field on the detector screen is (11)

$$\mathbf{E}_{\text{scr}}(\mathbf{r}) = \frac{ie^{ikr}}{2\pi r} k\hat{\mathbf{f}} \times \left[\int_{\text{aperture}} \hat{\mathbf{n}}' \times \mathbf{E}_{\text{far}}(\mathbf{r}') e^{-ik\hat{\mathbf{n}}' \cdot \mathbf{r}' + ik(r')^2/2r} da' \right] \quad (12)$$

where the subscript "scr" means the detector screen, $\hat{\mathbf{f}}$ is a unit vector along \mathbf{r} , a vector that points from the center of the lens to the image point on the detector screen (see Fig. 1), r is the magnitude of \mathbf{r} , and $\hat{\mathbf{n}}'$ is a unit vector normal to the lens plane. Since we set the lens plane and the detector screen to be parallel to the xy -plane, $\hat{\mathbf{n}}'$ is along the z -axis. The integration in Eq. 12 is over the surface of the lens aperture and accounts for all interference between the polarized wavelets, which form a polarization-dependent image on the detector screen. To simplify the integration, we make several further approximations. First, we neglect r' appearing in Eq. 10, since we consider only the paraxial rays, that is $r_0 \gg r'$. With this simplification, $\mathbf{P}(\mathbf{r}') = P(\mathbf{1} - \hat{\mathbf{x}}_0 \hat{\mathbf{x}}_0)$, where $\hat{\mathbf{x}}_0$ is a unit vector along \mathbf{x}_0 . And the tensor $\mathbf{1} - \hat{\mathbf{R}}_0 \hat{\mathbf{R}}_0$, which appears in Eq. 9, becomes $\mathbf{1} - \hat{\mathbf{x}}_0 \hat{\mathbf{x}}_0$. By the same reasoning, R_0 and $\hat{\mathbf{R}}_0$ are approximately equal to r_0 and \mathbf{R}_0/r_0 , so that Eq. 9 becomes

$$\mathbf{E}_{\text{scatt}}(\mathbf{r}') \approx \frac{k^2 e^{ikr_0}}{r_0} (\mathbf{1} - \hat{\mathbf{x}}_0 \hat{\mathbf{x}}_0) \cdot \sum_i e^{-ik\mathbf{R}_0/r_0 \cdot \mathbf{r}_i} \alpha_i \cdot E_0 e^{i\mathbf{k}_0 \cdot \mathbf{x}_i} \hat{\mathbf{e}}_0.$$

And the final equation of the electric field on the far face

of the lens, which is to be substituted into Eq. 12, is

$$\begin{aligned} \mathbf{E}_{\text{far,D}}(\mathbf{r}') &= P(\mathbf{1} - \hat{\mathbf{x}}_0 \hat{\mathbf{x}}_0) \exp \left\{ i \left[kn\Delta_0 - \frac{k(r')^2}{2f} \right] \right\} \frac{k^2 e^{ikr_0}}{r_0} \\ &\cdot (\mathbf{1} - \hat{\mathbf{x}}_0 \hat{\mathbf{x}}_0) \cdot \sum_i \exp \left(-ik \frac{\mathbf{R}_0}{r_0} \cdot \mathbf{r}_i \right) \alpha_i \\ &\cdot \hat{\mathbf{e}}_0 E_0 \exp(i\mathbf{k}_0 \cdot \mathbf{x}_i), \end{aligned} \quad (13)$$

where the subscript D indicates that this expression is valid for the dark-field geometry. Substituting Eq. 13 into Eq. 12 we obtain the expression of the electric field on the screen

$$\begin{aligned} \mathbf{E}_{\text{scr,D}}(\mathbf{r}) &= C' \hat{\mathbf{f}} \times \left(\hat{\mathbf{z}} \times (\mathbf{1} - \hat{\mathbf{x}}_0 \hat{\mathbf{x}}_0) \right. \\ &\cdot \sum_i \alpha_i e^{i\mathbf{k}(\hat{\mathbf{z}}_0 + \hat{\mathbf{k}}_0) \cdot \mathbf{r}_i} \left\{ \int_{\text{aperture}} \right. \\ &\cdot \exp i \left[\frac{k(r')^2}{2} \left(\frac{1}{r_0} + \frac{1}{r} - \frac{1}{f} \right) \right. \\ &\left. \left. - \left(\frac{k\mathbf{r}_i}{r_0} + k\hat{\mathbf{f}} \right) \cdot \mathbf{r}' \right] da' \right\} \cdot \hat{\mathbf{e}}_0 \left. \right), \end{aligned} \quad (14)$$

where

$$C' = \frac{iE_0 P k^3}{2\pi r r_0} e^{i\mathbf{k}(r+r_0+n\Delta_0+\hat{\mathbf{k}}_0 \cdot \mathbf{x}_0)}.$$

Notice that $(\mathbf{1} - \hat{\mathbf{x}}_0 \hat{\mathbf{x}}_0) \cdot (\mathbf{1} - \hat{\mathbf{x}}_0 \hat{\mathbf{x}}_0) = \mathbf{1} - \hat{\mathbf{x}}_0 \hat{\mathbf{x}}_0$. If we consider the image points on the detector screen near the lens axis, we find that, for these points, r is approximately equal to the distance between the lens and the detector screen, d . Then the quantity $1/r_0 + 1/r - 1/f$ appearing in Eq. 14 is zero according to the Gaussian lens formula $1/r_0 + 1/d - 1/f = 0$, which gives the exact position of the image point d for a given position of a point object at r_0 . The remaining integral in Eq. 14 is

$$\int_{\text{aperture}} \exp \left[-i \left(\frac{k\mathbf{r}_i}{r_0} + k\hat{\mathbf{f}} \right) \cdot \mathbf{r}' \right] da' = 2\pi a^2 \frac{J_1 \left(\frac{k a \rho_i}{r} \right)}{\left(\frac{k a \rho_i}{r} \right)}, \quad (15)$$

where J_1 is a Bessel function of the first kind of order 1, a is the radius of the lens, and $\rho_i = [(x + mx_i)^2 + (y + my_i)^2]^{1/2}$, where x and y are the components of \mathbf{r} , $m = d/r_0 \approx r/r_0$ is the magnification of the lens, and x_i and y_i are Cartesian components of \mathbf{r}_i . The derivation of Eq. 15 is shown in Appendix A.

Notice that the function $J_1(ka\rho_i/r)/(ka\rho_i/r)$ reaches a maximum when $x = -mx_i$ and $y = -my_i$, and diminishes for the nonzero values of ρ_i . It can be shown that the full-width at half-maximum of the principal maximum of the function $J_1(kax)/kax$ is equal to $4/ak = 2\lambda/(a\pi)$.

Therefore, the function $J_1(ka\rho_i/r)/(ka\rho_i/r)$ peaks more

sharply around the point where $\rho_i = 0$ as a gets larger or as the wavelength decreases. This gives one sharp image point at $(-mx_i, -my_i)$ for every source point at (x_i, y_i) .

Substituting Eq. 15 into Eq. 14, we obtain

$$\begin{aligned} \mathbf{E}_{\text{scr,D}}(\mathbf{r}) &= 2\pi a^2 C' \hat{\mathbf{f}} \times [\hat{\mathbf{z}} \times (\mathbf{1} - \hat{\mathbf{x}}_0 \hat{\mathbf{x}}_0) \\ &\cdot \sum_i \alpha_i e^{i\mathbf{k}(\hat{\mathbf{z}}_0 + \hat{\mathbf{k}}_0) \cdot \mathbf{r}_i} \frac{J_1 \left(\frac{k a \rho_i}{r} \right)}{\left(\frac{k a \rho_i}{r} \right)} \cdot \hat{\mathbf{e}}_0]. \end{aligned}$$

After some algebra, this equation becomes

$$\mathbf{E}_{\text{scr,D}}(\mathbf{r}) = 2\pi a^2 C' (\hat{\mathbf{z}} \hat{\mathbf{f}} - \hat{\mathbf{f}} \cdot \hat{\mathbf{z}}) \cdot \mathbf{F} \cdot \hat{\mathbf{e}}_0, \quad (16)$$

where

$$\mathbf{F} = \sum_i e^{-i\Delta \mathbf{k}' \cdot \mathbf{r}_i} \frac{J_1 \left(\frac{k a \rho_i}{r} \right)}{\left(\frac{k a \rho_i}{r} \right)} \alpha_i$$

and

$$\Delta \mathbf{k}' = k(-\hat{\mathbf{x}}_0 - \hat{\mathbf{k}}_0) = k(\hat{\mathbf{z}} - \hat{\mathbf{k}}_0)$$

is the momentum transfer vector. The detailed derivation of Eq. 16 is shown in Appendix B. Now, let us assume that an analyzer is placed between the lens and the detector screen to select the polarization component of the light that will contribute to the image. Mathematically this can be described as the dot product of a unit vector which represents the analyzer with $\mathbf{E}_{\text{scr,D}}(\mathbf{r})$ (Eq. 16) as follows:

$$E_{\text{scr,D}}(\mathbf{r}) = 2\pi a^2 C' (\hat{\mathbf{e}}^0)^* \cdot (\hat{\mathbf{z}} \hat{\mathbf{f}} - \hat{\mathbf{f}} \cdot \hat{\mathbf{z}}) \cdot \mathbf{F} \cdot \hat{\mathbf{e}}_0, \quad (17)$$

where $E_{\text{scr,D}}(\mathbf{r})$ is the amplitude of the electric field passing through the analyzer $\hat{\mathbf{e}}^0$ and arriving at \mathbf{r} on the screen, and the asterisk represents complex conjugation. Here we assume the analyzer to be ideal so that its transmittance along the permissive axis is 1. Notice that the unit vector describing the analyzer is labeled by a superscript while that of the incident polarizer is labeled by a subscript.

To obtain the image intensities appearing in the formulas of the first row in Table I, we square $E_{\text{scr,D}}(\mathbf{r})$ (Eq. 16). Then the image intensity is written

$$\begin{aligned} I_D(\mathbf{r}) &= \frac{c}{8\pi} \mathbf{E}_{\text{scr,D}}^*(\mathbf{r}) \cdot \mathbf{E}_{\text{scr,D}}(\mathbf{r}) \\ &= C'' \sum_i \sum_j \left[\frac{J_1 \left(\frac{k a \rho_i}{r} \right)}{\frac{k a \rho_i}{r}} \right] \left[\frac{J_1 \left(\frac{k a \rho_j}{r} \right)}{\frac{k a \rho_j}{r}} \right] e^{-i\Delta \mathbf{k}' \cdot \mathbf{r}_{ij}} \\ &\cdot \{ \hat{\mathbf{e}}_0^* \cdot \alpha_i^* \cdot [(\hat{\mathbf{f}} \cdot \hat{\mathbf{z}})^2 \mathbf{1} - (\hat{\mathbf{f}} \cdot \hat{\mathbf{z}})(\hat{\mathbf{f}} \hat{\mathbf{z}} + \hat{\mathbf{z}} \hat{\mathbf{f}}) + \hat{\mathbf{f}} \hat{\mathbf{f}}] \\ &\cdot \alpha_j \cdot \hat{\mathbf{e}}_0 \} \\ &= C'' \{ \hat{\mathbf{e}}_0^* \cdot \mathbf{F}^\dagger \cdot [(\hat{\mathbf{f}} \cdot \hat{\mathbf{z}})^2 \mathbf{1} - (\hat{\mathbf{f}} \cdot \hat{\mathbf{z}})(\hat{\mathbf{f}} \hat{\mathbf{z}} + \hat{\mathbf{z}} \hat{\mathbf{f}}) \\ &+ \hat{\mathbf{f}} \hat{\mathbf{f}}] \cdot \mathbf{F} \cdot \hat{\mathbf{e}}_0 \}, \end{aligned} \quad (18)$$

where \mathbf{F} is defined as in Eq. 16, $C'' = \pi c/2|a^2 C'|^2$, and $\mathbf{r}_{ij} = \mathbf{r}_j - \mathbf{r}_i$ is the distance vector between the groups i and j . $\hat{\epsilon}_0^*$ is the complex conjugate of $\hat{\epsilon}_0$ and α_i^\dagger is the conjugate transpose of α_i . This intensity is in cgs units and c is the speed of light.

The image intensities appearing in the rest of the elements in Table I are obtained by squaring Eq. 17:

$$\begin{aligned}
I_D(\mathbf{r}) &= \frac{c}{8\pi} [E_{\text{scr,D}}(\mathbf{r})]^* [E_{\text{scr,D}}(\mathbf{r})] \\
&= C'' \sum_i \sum_j \left[\frac{J_1\left(\frac{k\rho_i}{r}\right)}{\frac{k\rho_i}{r}} \right] \left[\frac{J_1\left(\frac{k\rho_j}{r}\right)}{\frac{k\rho_j}{r}} \right] e^{-i\Delta\mathbf{k}\cdot\mathbf{r}_{ij}} \\
&\quad [\hat{\epsilon}_0^* \cdot \alpha_i^\dagger \cdot (\hat{\mathbf{f}}\hat{\mathbf{z}} - \hat{\mathbf{f}} \cdot \hat{\mathbf{z}}) \cdot \hat{\epsilon}^0][(\hat{\epsilon}^0)^* \\
&\quad \cdot (\hat{\mathbf{z}}\hat{\mathbf{f}} - \hat{\mathbf{f}} \cdot \hat{\mathbf{z}}) \cdot \alpha_j \cdot \hat{\epsilon}_0] \\
&= C'' [\hat{\epsilon}_0^* \cdot \mathbf{F}^\dagger \cdot (\hat{\mathbf{f}}\hat{\mathbf{z}} - \hat{\mathbf{f}} \cdot \hat{\mathbf{z}}) \cdot \hat{\epsilon}^0] \\
&\quad \cdot [(\hat{\epsilon}^0)^* \cdot (\hat{\mathbf{z}}\hat{\mathbf{f}} - \hat{\mathbf{f}} \cdot \hat{\mathbf{z}}) \cdot \mathbf{F} \cdot \hat{\epsilon}_0], \quad (19)
\end{aligned}$$

where $(\hat{\epsilon}^0)^*$ is the complex conjugate of $\hat{\epsilon}^0$. Notice that Eqs. 18 and 19 contain the terms that are proportional to $[J_1(k\rho_i/r)/k\rho_i/r][J_1(k\rho_j/r)/k\rho_j/r]$. This function with $i = j$ characterizes the diffraction pattern in the neighborhood of the geometrical image of the i th group inside the sample. It has its principal maximum of $1/2$ at $k\rho_i/r = 0$, and with increasing $k\rho_i/r$ values it oscillates with gradually diminishing amplitude. Since the first minimum of the diffraction pattern of the i th point occurs when $\rho_i/r = 0.61 \lambda/a$, it can be shown that the resolution length Λ is given by (15)

$$\Lambda = 0.61 \frac{\lambda_0}{n \sin \theta},$$

where λ_0 is the wavelength of light in a vacuum, n is the refractive index of the medium in which the lens is immersed, and θ is the angle made by a marginal ray with the lens axis. Using the Gaussian lens formula $1/r_0 + 1/d = 1/f$, the above equation can be rewritten as

$$\Lambda = 0.61 \frac{\lambda_0}{n} \left\{ \left[\frac{r_0 f (m+1)^2}{am} \right]^2 + 1 \right\}^{1/2}.$$

From this equation, it can be easily seen that the resolving power, $1/\Lambda$, is poor when the paraxial approximation ($r_0 \gg a$) is used.¹ Also notice that, when the lens aperture becomes infinitely large, the imaging system is diffraction

¹This conclusion appears to be more restrictive than necessary. Indeed, experiments using a real microscope optics (see paper III) seem to indicate that the polarization of the light is not substantially altered even when using higher numerical aperture objectives. Thus, we have somewhat relaxed this restriction in performing the calculations presented in this series (see paper II). Nonetheless, this point certainly requires further theoretical attention to establish ultimately the limitations of the theory.

limited, and it attains the limit resolution length of $0.61 \lambda_0/n$.

The product of the first order Bessel functions with $i \neq j$ in Eqs. 18 and 19 characterizes the interference between the diffraction patterns of the i th and the j th group on the image plane. When the distance between the groups i and j is larger than the resolution length Λ , the cross terms ($i \neq j$) appearing in Eqs. 18 and 19 are negligible and only the terms with $i = j$ will contribute to the image. In this case, the image appears as a collection of well-resolved image points. When the distance between the groups i and j is just below the resolution length of the imaging device, the cross terms in Eqs. 18 and 19 contribute to the image significantly appearing as "bridges" between the image points of the groups i and j .

4. Mueller Image Entries. To obtain the M_{ij} ($j = 1, 2, 3, 4$) images, where no analyzer is present in the optical train, we simply choose the appropriate polarization unit vectors for $\hat{\epsilon}_0^*$ and $\hat{\epsilon}_0$ in Eq. 18, and combine the intensities according to the formulas of the first row in Table I. Throughout this section, the expressions for the Mueller entries will correspond to the numerators in Table I and, for simplicity, will not be normalized. For the rest of the Mueller images M_{ij} ($i = 2, 3, 4, j = 1, 2, 3, 4$), both the appropriate polarization unit vectors for polarizers ($\hat{\epsilon}_0, \hat{\epsilon}_0^*$) and analyzers ($\hat{\epsilon}^0, \hat{\epsilon}^{0*}$) must be used in Eq. 19 and the intensities obtained from Eq. 19 should be combined according to Table I.

To simplify the expressions so obtained, we notice that, for the elements of the last column and the last row of the Mueller matrix, M_{i4} and M_{4j} , ($i, j = 1, 2, 3, 4$) we can use the fact that $\hat{\epsilon}_L = \hat{\epsilon}_R^*$ and $\hat{\epsilon}^L = (\hat{\epsilon}^R)^*$, where $\hat{\epsilon}_L$ and $\hat{\epsilon}_R$ are the polarization unit vectors for the incident left and right circularly polarized light, respectively, and $\hat{\epsilon}^L$ and $\hat{\epsilon}^R$ are the unit vectors representing the corresponding quarter-wave plates. These identities cannot be used for the other elements and therefore we divide the 16 Mueller images into two classes.

□ CLASS I: M_{i4} AND M_{4j} ($i, j = 1, 2, 3, 4$) As an example of the derivation of the elements in this class we will show the derivation steps for M_{14} .

$$\begin{aligned}
M_{14} &= A \{ [(\hat{\mathbf{z}}\hat{\mathbf{f}} - \hat{\mathbf{f}} \cdot \hat{\mathbf{z}}) \cdot \mathbf{F} \cdot \hat{\epsilon}_R]^* \cdot [(\hat{\mathbf{z}}\hat{\mathbf{f}} - \hat{\mathbf{f}} \cdot \hat{\mathbf{z}}) \cdot \mathbf{F} \cdot \hat{\epsilon}_R] \\
&\quad - [(\hat{\mathbf{z}}\hat{\mathbf{f}} - \hat{\mathbf{f}} \cdot \hat{\mathbf{z}}) \cdot \mathbf{F} \cdot \hat{\epsilon}_L]^* \cdot [(\hat{\mathbf{z}}\hat{\mathbf{f}} - \hat{\mathbf{f}} \cdot \hat{\mathbf{z}}) \cdot \mathbf{F} \cdot \hat{\epsilon}_L] \} \\
&= A \{ \hat{\epsilon}_L \cdot \mathbf{F}^\dagger \cdot (\hat{\mathbf{f}}\hat{\mathbf{z}} - \hat{\mathbf{f}} \cdot \hat{\mathbf{z}}) \cdot (\hat{\mathbf{z}}\hat{\mathbf{f}} - \hat{\mathbf{f}} \cdot \hat{\mathbf{z}}) \cdot \mathbf{F} \cdot \hat{\epsilon}_R \\
&\quad - \hat{\epsilon}_R \cdot \mathbf{F}^\dagger \cdot (\hat{\mathbf{f}}\hat{\mathbf{z}} - \hat{\mathbf{f}} \cdot \hat{\mathbf{z}}) \cdot (\hat{\mathbf{z}}\hat{\mathbf{f}} - \hat{\mathbf{f}} \cdot \hat{\mathbf{z}}) \cdot \mathbf{F} \cdot \hat{\epsilon}_L \}, \quad (20)
\end{aligned}$$

where $A = (1/2I_0) C''$. The quantity $(\hat{\mathbf{f}}\hat{\mathbf{z}} - \hat{\mathbf{f}} \cdot \hat{\mathbf{z}}) \cdot (\hat{\mathbf{z}}\hat{\mathbf{f}} - \hat{\mathbf{f}} \cdot \hat{\mathbf{z}})$ can be expanded as a sum of dyadics:

$$\begin{aligned}
(\hat{\mathbf{f}}\hat{\mathbf{z}} - \hat{\mathbf{f}} \cdot \hat{\mathbf{z}}) \cdot (\hat{\mathbf{z}}\hat{\mathbf{f}} - \hat{\mathbf{f}} \cdot \hat{\mathbf{z}}) &= \hat{\mathbf{f}}\hat{\mathbf{f}} - (\hat{\mathbf{f}} \cdot \hat{\mathbf{z}})(\hat{\mathbf{f}}\hat{\mathbf{z}} + \hat{\mathbf{z}}\hat{\mathbf{f}}) + (\hat{\mathbf{f}} \cdot \hat{\mathbf{z}})^2 \mathbf{1} \\
&= \hat{\mathbf{f}}\hat{\mathbf{f}} - (\hat{\mathbf{f}} \cdot \hat{\mathbf{z}})(\hat{\mathbf{f}}\hat{\mathbf{z}} + \hat{\mathbf{z}}\hat{\mathbf{f}}) + (\hat{\mathbf{f}} \cdot \hat{\mathbf{z}})^2 (\hat{\mathbf{x}}\hat{\mathbf{x}} + \hat{\mathbf{y}}\hat{\mathbf{y}} + \hat{\mathbf{z}}\hat{\mathbf{z}}).
\end{aligned}$$

We may therefore gather the terms of Eq. 20 into a sum of

terms of the form

$$[\hat{\epsilon}_L \cdot (\mathbf{F}^\dagger \cdot \hat{\mathbf{a}})][(\hat{\mathbf{b}} \cdot \mathbf{F}) \cdot \hat{\epsilon}_R] - [\hat{\epsilon}_R \cdot (\mathbf{F}^\dagger \cdot \hat{\mathbf{a}})][(\hat{\mathbf{b}} \cdot \mathbf{F}) \cdot \hat{\epsilon}_L].$$

We can simplify this type of term by using a well-known vector identity, so that Eq. 20 becomes

$$M_{14} = -iA(\mathbf{F} \times \mathbf{F}^\dagger)_{\alpha\beta\gamma}[(\hat{\mathbf{r}} \cdot \hat{\mathbf{z}})^2 - (\hat{\mathbf{r}} \cdot \hat{\mathbf{z}})(\hat{\mathbf{r}}\hat{\mathbf{z}} + \hat{\mathbf{z}}\hat{\mathbf{r}}) + \hat{\mathbf{r}}\hat{\mathbf{r}}]_{\alpha\gamma}\hat{\mathbf{k}}_{0\beta}. \quad (21a)$$

To arrive at Eq. 21a, we have used $\hat{\epsilon}_R = 1/\sqrt{2}(\hat{\epsilon}_H + i\hat{\epsilon}_V)$ and $\hat{\epsilon}_L = 1/\sqrt{2}(\hat{\epsilon}_H - i\hat{\epsilon}_V)$, where $\hat{\epsilon}_H$ and $\hat{\epsilon}_V$ are the polarization unit vectors for the incident horizontal and vertical polarization of light. Similarly the rest of M_{i4} and M_{4i} are

$$M_{24} = -iA(\hat{\mathbf{r}} \cdot \hat{\mathbf{z}})^2(\mathbf{F} \times \mathbf{F}^\dagger)_{\alpha\beta\gamma}(\hat{\epsilon}_\alpha^H\hat{\epsilon}_\gamma^H - \hat{\epsilon}_\alpha^V\hat{\epsilon}_\gamma^V)\hat{\mathbf{k}}_{0\beta} \quad (21b)$$

$$M_{34} = -iA(\hat{\mathbf{r}} \cdot \hat{\mathbf{z}})^2(\mathbf{F} \times \mathbf{F}^\dagger)_{\alpha\beta\gamma}(\hat{\epsilon}_\alpha^H\hat{\epsilon}_\gamma^V + \hat{\epsilon}_\alpha^V\hat{\epsilon}_\gamma^H)\hat{\mathbf{k}}_{0\beta} \quad (21c)$$

$$M_{44} = A(\hat{\mathbf{r}} \cdot \hat{\mathbf{z}})^2(\mathbf{F} \times \mathbf{F}^\dagger)_{\alpha\beta\gamma}(\hat{\epsilon}_\alpha^H\hat{\epsilon}_\gamma^V - \hat{\epsilon}_\alpha^V\hat{\epsilon}_\gamma^H)\hat{\mathbf{k}}_{0\beta} \quad (21d)$$

$$M_{41} = -iA(\hat{\mathbf{r}} \cdot \hat{\mathbf{z}})^2(\mathbf{F}^\dagger \times \mathbf{F})_{\alpha\beta\gamma}(\mathbf{I} - \hat{\mathbf{k}}_0\hat{\mathbf{k}}_0)_{\alpha\gamma}\hat{\mathbf{z}}_\beta \quad (21e)$$

$$M_{42} = -iA(\hat{\mathbf{r}} \cdot \hat{\mathbf{z}})^2(\mathbf{F}^\dagger \times \mathbf{F})_{\alpha\beta\gamma}(\hat{\epsilon}_{H\alpha}\hat{\epsilon}_{H\gamma} - \hat{\epsilon}_{V\alpha}\hat{\epsilon}_{V\gamma})\hat{\mathbf{z}}_\beta \quad (21f)$$

$$M_{43} = -iA(\hat{\mathbf{r}} \cdot \hat{\mathbf{z}})^2(\mathbf{F}^\dagger \times \mathbf{F})_{\alpha\beta\gamma}(\hat{\epsilon}_{H\alpha}\hat{\epsilon}_{V\gamma} + \hat{\epsilon}_{V\alpha}\hat{\epsilon}_{H\gamma})\hat{\mathbf{z}}_\beta, \quad (21g)$$

where repeated indices imply a summation, and $\hat{\epsilon}^H$ and $\hat{\epsilon}^V$ are the unit vectors, which represent the analyzers placed between the lens and the screen. The superscripts H and V mean horizontal and vertical with reference to an arbitrary set of laboratory coordinates. The quantity $(\mathbf{F} \times \mathbf{F}^\dagger)_{\alpha\beta\gamma}$ is the cross product of two second rank tensors and is defined as

$$(\mathbf{F} \times \mathbf{F}^\dagger)_{\alpha\beta\gamma} = \epsilon_{\beta\delta\eta}F_{\alpha\delta}F_{\eta\gamma}^\dagger,$$

where the symbol $\epsilon_{\beta\delta\eta}$ represents the Levi-Civita tensor. The tensor $(\mathbf{F} \times \mathbf{F}^\dagger)_{\alpha\beta\gamma}$ is expanded as follows:

$$(\mathbf{F} \times \mathbf{F}^\dagger)_{\alpha\beta\gamma} = \sum_i \sum_j \left[\frac{J_1\left(\frac{k\rho_i}{r}\right)}{\frac{k\rho_i}{r}} \right] \left[\frac{J_1\left(\frac{k\rho_j}{r}\right)}{\frac{k\rho_j}{r}} \right] \cdot e^{-i\Delta\mathbf{k} \cdot \mathbf{r}_{ij}} (\alpha_i \times \alpha_j)_{\alpha\beta\gamma}. \quad (22a)$$

Two different cases will be considered in connection with this expression. First, let's consider the special case when all image points are well resolved. In this case, the cross terms in Eqs. 22a vanish and we obtain

$$(\mathbf{F} \times \mathbf{F}^\dagger)_{\alpha\beta\gamma} = \sum_i \left[\frac{J_1\left(\frac{k\rho_i}{r}\right)}{\frac{k\rho_i}{r}} \right]^2 (\alpha_i \times \alpha_i)_{\alpha\beta\gamma}. \quad (22b)$$

This result is valid for Eqs. 21a–g all of which are sensitive to the chirality of the object. The meaning of this result is straightforward: since the phenomenon of preferential scattering of right vs. left circularly polarized light, also

known as CIDS (16–18) is an interference phenomenon, it appears as the result of the interference of the wavelets scattered by groups that bear a chiral relationship with one another. When the imaging system resolves the individual groups, their interference contribution in the image vanish and only the intrinsic optical activity effects survive. The contribution of these intrinsic optical effects can be seen from the fact that the limitations imposed on the spatial resolution of an optical system by the finite dimension of the wavelength of the light (diffraction-limited resolution) determine the smallest size of the point-polarizable groups into which the object can be partitioned. Since the volume of such groups is of the order of λ (3), it follows that each polarizable group represents a large number of smaller point polarizable elements whose dimensions are beyond the resolution of the optical system. Despite this fact, these smaller elements do affect the overall image since they give rise to the intrinsic optical properties displayed by the larger groups. As a result of this, when the larger groups are well resolved in the image, Eq. 22b shows that the M_{i4} and M_{4j} ($i, j = 1, 2, 3, 4$) images appear as a collection of localized points, each of them having associated with them a positive or a negative differential scattering intensity related to the intrinsic optical activity of the individual groups, and given by

$$\alpha_i \times \alpha_i^\dagger.$$

In the case of the M_{i4} images, this optical activity contains contributions from CIDS and, if the incident wavelength falls inside an absorption band, these scattering terms carry information about the circular dichroism of the individual groups. This can be termed scattering-detected circular dichroism. The M_{24} , M_{34} , and M_{44} images describe the excess of certain polarization components in the light scattered between right and left circularly polarized incident light. The M_{41} , M_{42} , and M_{43} images display the ability of these individual groups to introduce circularity in the scattered light when the object is illuminated with unpolarized light (M_{41}) or display the excess of circularity of one sense over the other introduced in the scattered light between two incident orthogonal linear polarizations (M_{42} and M_{43}).

On the other hand, if the images are displayed at a resolution below that required to resolve the individual groups and if the dipole moments induced in these groups bear a chiral relation to each other, the M_{4j} and M_{i4} images ($i, j = 1, 2, 3, 4$) contain the contributions of the intrinsic optical activity of the groups as well as that resulting from the chiral arrangement of the groups, i.e., CIDS. The latter corresponds to the overlapping of the image points as given by the cross terms in Eq. 22a.

□ CLASS II: M_{ij} ($i, j = 1, 2, 3$) The derivation of the rest of the Mueller images does not involve any particular mathematical subtleties and is straightforward. Therefore

we simply write the final equations below:

$$M_{11} = A\Gamma_{\alpha\beta} (\mathbf{I} - \hat{\mathbf{k}}_0\hat{\mathbf{k}}_0)_{\alpha\beta} \quad (23a)$$

$$M_{12} = A\Gamma_{\alpha\beta} (\hat{\epsilon}_{\text{Ha}}\hat{\epsilon}_{\text{H}\beta} - \hat{\epsilon}_{\text{v}\alpha}\hat{\epsilon}_{\text{v}\beta}) \quad (23b)$$

$$M_{13} = A\Gamma_{\alpha\beta} (\hat{\epsilon}_{\text{Ha}}\hat{\epsilon}_{\text{v}\beta} + \hat{\epsilon}_{\text{v}\alpha}\hat{\epsilon}_{\text{H}\beta}) \quad (23c)$$

$$M_{21} = A(\hat{\mathbf{r}} \cdot \hat{\mathbf{z}})^2 [\mathbf{F}^\dagger \cdot (\hat{\epsilon}^{\text{H}}\hat{\epsilon}^{\text{H}} - \hat{\epsilon}^{\text{V}}\hat{\epsilon}^{\text{V}}) \cdot \mathbf{F}]_{\alpha\beta} (\mathbf{I} - \hat{\mathbf{k}}_0\hat{\mathbf{k}}_0)_{\alpha\beta} \quad (23d)$$

$$M_{22} = A(\hat{\mathbf{r}} \cdot \hat{\mathbf{z}})^2 [\mathbf{F}^\dagger \cdot (\hat{\epsilon}^{\text{H}}\hat{\epsilon}^{\text{H}} - \hat{\epsilon}^{\text{V}}\hat{\epsilon}^{\text{V}}) \cdot \mathbf{F}]_{\alpha\beta} \cdot (\hat{\epsilon}_{\text{Ha}}\hat{\epsilon}_{\text{H}\beta} - \hat{\epsilon}_{\text{v}\alpha}\hat{\epsilon}_{\text{v}\beta}) \quad (23e)$$

$$M_{23} = A(\hat{\mathbf{r}} \cdot \hat{\mathbf{z}})^2 [\mathbf{F}^\dagger \cdot (\hat{\epsilon}^{\text{H}}\hat{\epsilon}^{\text{H}} - \hat{\epsilon}^{\text{V}}\hat{\epsilon}^{\text{V}}) \cdot \mathbf{F}]_{\alpha\beta} \cdot (\hat{\epsilon}_{\text{Ha}}\hat{\epsilon}_{\text{v}\beta} + \hat{\epsilon}_{\text{v}\alpha}\hat{\epsilon}_{\text{H}\beta}) \quad (23f)$$

$$M_{31} = A(\hat{\mathbf{r}} \cdot \hat{\mathbf{z}})^2 [\mathbf{F}^\dagger \cdot (\hat{\epsilon}^{\text{H}}\hat{\epsilon}^{\text{V}} + \hat{\epsilon}^{\text{V}}\hat{\epsilon}^{\text{H}}) \cdot \mathbf{F}]_{\alpha\beta} (\mathbf{I} - \hat{\mathbf{k}}_0\hat{\mathbf{k}}_0)_{\alpha\beta} \quad (23g)$$

$$M_{32} = A(\hat{\mathbf{r}} \cdot \hat{\mathbf{z}})^2 [\mathbf{F}^\dagger \cdot (\hat{\epsilon}^{\text{H}}\hat{\epsilon}^{\text{V}} + \hat{\epsilon}^{\text{V}}\hat{\epsilon}^{\text{H}}) \cdot \mathbf{F}]_{\alpha\beta} \cdot (\hat{\epsilon}_{\text{Ha}}\hat{\epsilon}_{\text{H}\beta} - \hat{\epsilon}_{\text{v}\alpha}\hat{\epsilon}_{\text{v}\beta}) \quad (23h)$$

$$M_{33} = A(\hat{\mathbf{r}} \cdot \hat{\mathbf{z}})^2 [\mathbf{F}^\dagger \cdot (\hat{\epsilon}^{\text{H}}\hat{\epsilon}^{\text{V}} + \hat{\epsilon}^{\text{V}}\hat{\epsilon}^{\text{H}}) \cdot \mathbf{F}]_{\alpha\beta} (\hat{\epsilon}_{\text{Ha}}\hat{\epsilon}_{\text{v}\beta} + \hat{\epsilon}_{\text{v}\alpha}\hat{\epsilon}_{\text{H}\beta}), \quad (23i)$$

where

$$\begin{aligned} \Gamma &= \mathbf{F}^\dagger \cdot (\hat{\mathbf{r}}\hat{\mathbf{z}} - \hat{\mathbf{r}} \cdot \hat{\mathbf{z}}) \cdot (\hat{\mathbf{z}}\hat{\mathbf{r}} - \hat{\mathbf{r}} \cdot \hat{\mathbf{z}}) \cdot \mathbf{F} \\ &= \sum_i \sum_j \left[\frac{J_1\left(\frac{k\rho_i}{r}\right)}{\frac{k\rho_i}{r}} \right] \left[\frac{J_1\left(\frac{k\rho_j}{r}\right)}{\frac{k\rho_j}{r}} \right] \\ &\quad \cdot e^{-i\Delta\mathbf{k} \cdot \mathbf{r}} \alpha_i^\dagger \cdot (\hat{\mathbf{r}}\hat{\mathbf{z}} - \hat{\mathbf{r}} \cdot \hat{\mathbf{z}}) \cdot (\hat{\mathbf{z}}\hat{\mathbf{r}} - \hat{\mathbf{r}} \cdot \hat{\mathbf{z}}) \cdot \alpha_j. \end{aligned}$$

Notice that M_{11} contain the tensor $(\mathbf{I} - \hat{\mathbf{k}}_0\hat{\mathbf{k}}_0)_{\alpha\beta}$, which indicates the fact that M_{11} images are obtained using unpolarized incident light. Also the tensors $(\hat{\epsilon}_{\text{Ha}}\hat{\epsilon}_{\text{H}\beta} - \hat{\epsilon}_{\text{v}\alpha}\hat{\epsilon}_{\text{v}\beta})$ and $(\hat{\epsilon}_{\text{Ha}}\hat{\epsilon}_{\text{v}\beta} + \hat{\epsilon}_{\text{v}\alpha}\hat{\epsilon}_{\text{H}\beta})$ appear in the equations of M_{12} and of M_{13} , respectively. This indicates that M_{12} and M_{13} images are obtained using pairs of horizontal and vertical, and $+45^\circ$ and -45° polarization of incident light, respectively. The dyadics $\hat{\epsilon}^{\text{H}}\hat{\epsilon}^{\text{H}} - \hat{\epsilon}^{\text{V}}\hat{\epsilon}^{\text{V}}$ in the equations of M_{21} and $\hat{\epsilon}^{\text{H}}\hat{\epsilon}^{\text{V}} + \hat{\epsilon}^{\text{V}}\hat{\epsilon}^{\text{H}}$ in the equations of M_{31} indicate the fact that pairs of horizontal and vertical, and $+45^\circ$ and -45° analyzers are used to obtain M_{21} and M_{31} , respectively.

In general, the 16 Mueller images of an arbitrarily oriented object are all different from each other in dark-field imaging. However, there are seven independent parameters and nine relations between the 16 Mueller matrix elements (8). These relations, which also hold for the imaging case, are derived explicitly by Abhyankar et al. (19).

Experimentally, it is convenient to normalize all the Mueller matrix entries, dividing them by the sum of the intensities appearing in the numerator. In this way, the Mueller images become bi-dimensional maps of the relative efficiency of the different parts of the object to interact preferentially with the incident polarizations of light. With this normalization, the observer can compare the values of distinct domains in a given Mueller image without regard

to the differences in absorption or scattering cross-sections between these domains.

C. Bright-Field Equations

In the bright-field geometry, absorption is the dominant phenomenon. Therefore, the absorption of the incident light by the sample must be explicitly described in bright-field imaging. In classical electrodynamics theory, absorption by an object is described as interference between the incident electric field and the electric field scattered by that object (11). Therefore, the bright-field equation of the electric field on the near face of the lens is written:

$$\mathbf{E}_{\text{near}}(\mathbf{r}') = E_0\hat{\epsilon}_0 e^{i\mathbf{k}_0 \cdot \mathbf{r}'} + \mathbf{E}_{\text{scatt}}(\mathbf{r}'), \quad (24)$$

where E_0 , $\hat{\epsilon}_0$, and \mathbf{k}_0 are the amplitude, the polarization unit vector, and the wave vector of the incident light, respectively. To obtain the electric field on the far face of the lens, we substitute Eq. 24 into Eq. 11. Then, we obtain

$$\begin{aligned} \mathbf{E}_{\text{far,B}}(\mathbf{r}') &= P(\mathbf{I} - \hat{\mathbf{x}}_0\hat{\mathbf{x}}_0) \cdot \exp\left[i\left(kn\Delta_0 - \frac{k(r')^2}{2f}\right)\right] \\ &\quad \cdot [E_0\hat{\epsilon}_0 \exp(i\mathbf{k}_0 \cdot \mathbf{r}') + \mathbf{E}_{\text{scatt}}(\mathbf{r}')], \quad (25) \end{aligned}$$

where the subscript B indicates the bright-field imaging.

To obtain the electric field on the image plane we substitute Eq. 25 into Eq. 12:

$$\begin{aligned} \mathbf{E}_{\text{scr,B}}(\mathbf{r}) &= \frac{ie^{ikr}}{2\pi r} k\hat{\mathbf{f}} \times \left\{ \int_{\text{aperture}} \hat{\mathbf{n}}' \times \left\{ P(\mathbf{I} - \hat{\mathbf{x}}_0\hat{\mathbf{x}}_0) \right. \right. \\ &\quad \cdot e^{i[kn\Delta_0 - k(r')^2/2f]} [E_0\hat{\epsilon}_0 e^{i\mathbf{k}_0 \cdot \mathbf{r}'} \\ &\quad \left. \left. + \mathbf{E}_{\text{scatt}}(\mathbf{r}') \right\} e^{-i\mathbf{k}\mathbf{t} \cdot \mathbf{r}' + i\mathbf{k}(r')^2/2r} d\alpha' \right\} \\ &= \frac{ie^{ikr}}{2\pi r} k\hat{\mathbf{f}} \times \left\{ \int_{\text{aperture}} \hat{\mathbf{n}}' \times [P(\mathbf{I} - \hat{\mathbf{x}}_0\hat{\mathbf{x}}_0) \right. \\ &\quad \cdot e^{i[kn\Delta_0 - k(r')^2/2f]} \\ &\quad \left. \cdot E_0\hat{\epsilon}_0 e^{i\mathbf{k}_0 \cdot \mathbf{r}'}] e^{-i\mathbf{k}\mathbf{t} \cdot \mathbf{r}' + i\mathbf{k}(r')^2/2r} d\alpha' \right\} + \mathbf{E}_{\text{scr,D}}(\mathbf{r}). \quad (26) \end{aligned}$$

Rearranging Eq. 26 gives

$$\begin{aligned} \mathbf{E}_{\text{scr,B}}(\mathbf{r}) &= C''' \mathbf{r} \times (\hat{\mathbf{z}} \times \hat{\epsilon}_0) \int_{\text{aperture}} e^{(1/2)ik(1/r-1/f)(r')^2} e^{-i\Delta\mathbf{k} \cdot \mathbf{r}'} d\alpha' \\ &\quad + \mathbf{E}_{\text{scr,D}}(\mathbf{r}), \quad (27) \end{aligned}$$

where

$$C''' = \frac{iPE_0k e^{ik(r+n\Delta_0)}}{2\pi r} \quad \text{and} \quad \Delta\mathbf{k} = k(\hat{\mathbf{z}} - \hat{\mathbf{k}}_0).$$

The integration in Eq. 27 is done by assuming the aperture to be square and infinitely wide. The result is

$$\begin{aligned} \mathbf{E}_{\text{scr,B}}(\mathbf{r}) &= C''' \hat{\mathbf{f}} \times (\hat{\mathbf{z}} \times \hat{\epsilon}_0) \left(-\frac{i2\pi r_0}{k} \right) \exp\left[\frac{ir_0k}{2r^2} (x^2 + y^2)\right] \\ &\quad + \mathbf{E}_{\text{scr,D}}(\mathbf{r}). \quad (28) \end{aligned}$$

The integration of Eq. 27 is shown in Appendix C. If the object being imaged has dimensions on the order of the wavelength of the incident light, then its image will have dimensions on the order of $m\lambda$. Then the exponent in Eq. 28 is

$$\frac{r_0 k}{2r^2} (x^2 + y^2) \approx \frac{r_0 k}{2r^2} (m\lambda)^2 = \pi m \left(\frac{\lambda}{r} \right).$$

In most situations, λ/r is very small so that $\pi m (\lambda/r) \ll 1$. Therefore, we can take the illumination of the screen by the incident wave to be virtually constant for the given wavelength of light:

$$\mathbf{E}_{\text{scr,B}}(\mathbf{r}) \approx -\frac{i2\pi r_0 C'''}{k} \hat{\mathbf{r}} \times (\hat{\mathbf{z}} \times \hat{\mathbf{e}}_0) + \mathbf{E}_{\text{scr,D}}(\mathbf{r}).$$

After some algebra (refer to Appendix B), we obtain

$$\begin{aligned} \mathbf{E}_{\text{scr,B}}(\mathbf{r}) &= -\frac{i2\pi r_0 C'''}{k} (\hat{\mathbf{z}}\hat{\mathbf{r}} - \hat{\mathbf{r}} \cdot \hat{\mathbf{z}}) \cdot \mathbf{I} \cdot \hat{\mathbf{e}}_0 + \mathbf{E}_{\text{scr,D}}(\mathbf{r}). \\ &= 2\pi a^2 C' (\hat{\mathbf{z}}\hat{\mathbf{r}} - \hat{\mathbf{r}} \cdot \hat{\mathbf{z}}) \cdot \hat{\mathbf{G}} \cdot \hat{\mathbf{e}}_0 \end{aligned} \quad (29)$$

where

$$\mathbf{G} = \frac{r_0^2}{ia^2 k^3} \mathbf{I} + \sum_i e^{-i\Delta\mathbf{k}' \cdot \mathbf{r}_i} \frac{J_1\left(\frac{k\rho_i}{r}\right) \alpha_i}{\frac{k\rho_i}{r}}.$$

To obtain the bright-field image intensities at each position on the detector screen, we square Eq. 29:

$$I_B(\mathbf{r}) = C'' \{ \hat{\mathbf{e}}_0^* \cdot \mathbf{G}^\dagger \cdot [(\hat{\mathbf{r}} \cdot \hat{\mathbf{z}})^2 - (\hat{\mathbf{r}} \cdot \hat{\mathbf{z}})(\hat{\mathbf{r}}\hat{\mathbf{z}} + \hat{\mathbf{z}}\hat{\mathbf{r}}) + \hat{\mathbf{r}}\hat{\mathbf{r}}] \cdot \mathbf{G} \cdot \hat{\mathbf{e}}_0 \} \quad (30)$$

where C'' is defined as before. The valid expression when an arbitrary analyzer is present can be obtained in a similar manner.

The spatial resolution for the bright-field Mueller images is identical to that already derived for the dark-field geometry, and its derivation will not be repeated here. Notice that the only difference between the equations of $I_D(\mathbf{r})$ (Eqs. 18 and 19) and $I_B(\mathbf{r})$ is that the \mathbf{F} tensor has been replaced by the \mathbf{G} tensor. Therefore, to obtain the bright-field Mueller images, we simply replace the tensors \mathbf{F} and \mathbf{F}^\dagger in the dark-field equations with the tensors \mathbf{G} and \mathbf{G}^\dagger . Thus, the bright-field equations can also be classified into two distinct classes. (Again, we present only the unnormalized expressions of the Mueller entries here.)

□ CLASS I: M_{i4} AND M_{4j} ($i, j = 1, 2, 3, 4$)

$$M_{14} = -iA(\mathbf{G} \times \mathbf{G}^\dagger)_{\alpha\beta\gamma} [(\hat{\mathbf{r}} \cdot \hat{\mathbf{z}})^2 \mathbf{I} - (\hat{\mathbf{r}} \cdot \hat{\mathbf{z}})(\hat{\mathbf{r}}\hat{\mathbf{z}} + \hat{\mathbf{z}}\hat{\mathbf{r}}) + \hat{\mathbf{r}}\hat{\mathbf{r}}]_{\alpha\gamma} \hat{\mathbf{k}}_{0\beta} \quad (31)$$

and so forth, according to the expressions 21b–21g.

□ CLASS II: M_{ij} ($i, j = 1, 2, 3$)

$$M_{11} = A\Gamma'_{\alpha\beta} (\mathbf{I} - \hat{\mathbf{k}}_0 \hat{\mathbf{k}}_0)_{\alpha\beta} \quad (32)$$

and so forth, according to Eqs. 23b–23i where $\Gamma' = \mathbf{G}^\dagger \cdot (\hat{\mathbf{r}}\hat{\mathbf{z}} - \hat{\mathbf{z}}\hat{\mathbf{r}}) \cdot (\hat{\mathbf{z}}\hat{\mathbf{r}} - \hat{\mathbf{r}}\hat{\mathbf{z}}) \cdot \mathbf{G}$.

In general, the bright-field equations include (a) the background illumination, (b) the extinction (scattering and absorption) effects, and (c) the forward scattering contributions. Here we will single out these contributions in the equations of Class I. To do this, we expand the tensor $\mathbf{G} \times \mathbf{G}^\dagger$ as

$$(\mathbf{G} \times \mathbf{G}^\dagger)_{\alpha\beta\gamma} = \left[\left(\frac{r_0^2}{a^2 k^3} \right)^2 \mathbf{I} \times \mathbf{I} + \frac{r_0^2}{ia^2 k^3} \cdot (\mathbf{I} \times \mathbf{F}^\dagger - \mathbf{F} \times \mathbf{I}) + \mathbf{F} \times \mathbf{F}^\dagger \right]_{\alpha\beta\gamma},$$

where

$$\mathbf{F} = \sum_i \frac{J_1\left(\frac{k\rho_i}{r}\right)}{\frac{k\rho_i}{r}} \alpha_i.$$

Notice that $\Delta\mathbf{k}' = \mathbf{0}$ in the forward direction.

The first term containing the tensor $(\mathbf{I} \times \mathbf{I})_{\alpha\beta\gamma}$ is the background illumination and it does not contribute to M_{4j} or M_{i4} with the exception of M_{44} . To illustrate this, we write the background illumination of M_{42} as follows:

$$\begin{aligned} -iA(\hat{\mathbf{r}} \cdot \hat{\mathbf{z}})^2 \left(\frac{r_0^2}{a^2 k^3} \right)^2 (\mathbf{I} \times \mathbf{I})_{\alpha\beta\gamma} (\hat{\mathbf{e}}_{H\alpha} \hat{\mathbf{e}}_{H\gamma} - \hat{\mathbf{e}}_{V\alpha} \hat{\mathbf{e}}_{V\gamma}) \hat{\mathbf{z}}_\beta \\ = -iA(\hat{\mathbf{r}} \cdot \hat{\mathbf{z}})^2 \left(\frac{r_0^2}{a^2 k^3} \right)^2 (\hat{\mathbf{e}}_H \times \hat{\mathbf{e}}_H - \hat{\mathbf{e}}_V \times \hat{\mathbf{e}}_V) \cdot \hat{\mathbf{z}}, \end{aligned}$$

which vanishes identically. In the M_{44} image, the illumination of the incident light is constant over the image plane for a given wavelength of the incident plane wave.

The second term, which is proportional to $(\mathbf{I} \times \mathbf{F}^\dagger - \mathbf{F} \times \mathbf{I})_{\alpha\beta\gamma}$ contains the extinction effects. This can be proved using the optical theorem (refer to Appendix D). In the case of M_{14} this second term is proportional to the differential power dissipated for right- and left-circularly polarized light, i.e., to the circular dichroism of each feature inside the sample. In the first Born-Approximation, this is the term that gives rise to the nonzero M_{14} bright-field image. However, if the polarizability tensor of each group is symmetric, this term becomes zero. Thus, to have a nonzero M_{14} bright-field image, the individual group must possess intrinsic optical activity as described in section B.1 of part II of this paper. For the images corresponding to the elements M_{i4} and M_{4j} ($i, j = 2, 3$) in bright-field imaging, this term is related to the linear birefringence of the sample. (Refer to paper II of this series.)

The third term containing $(\mathbf{F} \times \mathbf{F}^\dagger)_{\alpha\beta\gamma}$ is the forward differential scattering contribution and it cannot contribute at all to M_{i4} and M_{4j} in the first Born-Approximation when the incident wavelengths are outside the absorption bands of the groups and when each group is not optically

active, with the exception of M_{44} . This is because the forward differential scattering contribution to M_{i4} and M_{4j} (except M_{44}) requires the interference of the secondary wavelets generated at each group in the object. For an optically inactive medium in the first Born-Approximation, these wavelets cannot interfere in the forward direction and the forward differential scattering vanishes. Mathematically, we see from Eq. 22a that $(\mathbf{F} \times \mathbf{F}^\dagger)_{\alpha\beta\gamma}$ is antisymmetric with respect to an exchange in the subindices i and j and therefore the double summation involved in this expression cancels term by term.² Conversely, when the incident wavelengths are inside the absorption bands the group polarizabilities are complex and thus the double summation in $\mathbf{F} \times \mathbf{F}^\dagger$ can be split into two parts. The first, containing the products of the purely real and purely imaginary parts of the group polarizabilities, cancels out by the above arguments. The second part contains the interference effects between the absorptive and refractive properties of the group polarizabilities. This part does contribute to the Mueller images of Class I if the polarizable groups are not identical. However, its contribution is small compared with the power absorbed by the groups.

The above arguments allow us to arrive at the following conclusion: At the position of a well-resolved feature the bright-field circular differential image M_{14} reduces to approximately the circular dichroism of the feature. That is, the circular differential image M_{14} is essentially a map of the circular dichroism of each feature in the sample in the bright-field experiment.

When the object is optically dense, the transition dipoles induced at the groups interact with one another significantly. As a result, multiple scattering events take place as the light travels through the object, successively modifying its state of polarization. Thus, each polarizable group along the optical path will experience a field of different polarization. If the incident polarization is circular, it can be shown (20) that this mechanism can give rise to forward differential scattering contribution to the M_{i4} ($i = 1, 2, 3$) images. Similarly, the amount of circular components introduced in the incident linear polarizations by these multiple scattering effects will yield a forward differential scattering contribution to the M_{4j} ($j = 1, 2, 3$) images. This optically dense behavior of the images can be taken into account by higher Born-Approximations of the internal field.

The bright-field equations of Class II, M_{ij} ($i, j = 1, 2, 3$) also contain three contributions just as those of M_{i4} or M_{4j} ($i, j = 1, 2, 3, 4$), however, there is always a forward differential scattering contribution in M_{ij} ($i, j = 1, 2, 3$) images unlike in the images of Class I, which require optically dense materials (higher Born-Approximations). This is because the sign and the magnitude of each spot in the Mueller images of Class II are determined by the orientation of the dipole moments relative to the linear

polarization of the incident light, and do not require interference effects.

In Class II, the background illumination does not contribute to the M_{ij} ($i \neq j$) images, either. In general, the background illumination is cancelled out in M_{ij} ($i, j = 1, 2, 3, 4; i \neq j$), but it contributes to M_{ii} ($i = 1, 2, 3, 4$). This can be easily seen by looking at the diagonal entries in Table I. When there is no object, $I_H^H + I_V^V$ in M_{22} , $I_{+45}^{+45} + I_{-45}^{-45}$ in M_{33} , and $I_R^R + I_L^L$ in M_{44} are not cancelled out and are always equal to 1 after normalization.

Finally it should be mentioned that in the bright-field geometry, the incident direction $\hat{\mathbf{k}}_0$ coincides with the transmitted direction $\hat{\mathbf{z}}$ (see Fig. 1).

In the most general case of an optical medium that is both linearly and circularly anisotropic, there are only six independent parameters to be determined in bright-field (21, 22). Furthermore, special symmetry relationships between Mueller elements can be found in less general cases. These relationships are presented in the second paper of this series.

D. Range of Validity of the First Born-Approximation

The formulas derived throughout most of this paper have been obtained within the frame of the first Born-Approximation, in which the light is allowed to interact only once with the optical medium before it reaches the measuring device. This simplified view assumes that the dipoles are not coupled to one another and that the field in the medium (the internal field) can be approximated by the incident field. This approach is also referred to as the Rayleigh-Gans approximation in light scattering theory (8). The conditions under which this approximation is valid can be summarized as follows (8): (a) that the refractive index of the domain (n) differs only slightly from that of the surrounding medium (n_0):

$$|n - n_0| \ll 1,$$

and (b) that the phase shift of the wave in the medium is small:

$$kd|n - n_0| \ll 1$$

where $k = 2\pi/\lambda$, and d is the thickness of the optical medium.

The second of these conditions is more restrictive and imposes a condition on the thickness of the samples that can be treated within this approximation. In applications of microscopy to biological samples, $d \approx 1 \mu\text{m}$, $k \approx 10 (1/\mu\text{m})$, which requires that $|n - n_0| \ll .1$. This is a reasonable expectation in most biological samples, n_0 can be estimated to be equal to the index of refraction of water, and for unstained specimens the value of n is very close to n_0 . When the biological object absorbs substantially at the wavelength of the incident light, this condition might not be fulfilled.

²This is true when the polarizability tensor is symmetric.

Finally, operating under experimental conditions in which the first Born-Approximation is valid, will be more important in differential polarization imaging than in regular polarization spectroscopy in which the samples are rotationally averaged over multiple orientations. In the latter case, even though the light experiences multiple sequential interactions within the medium, the isotropy of the medium preserves the polarization of the light, substantially simplifying the interpretation of the Mueller elements. It can be seen that, in oriented systems, this condition will only be fulfilled in the first Born-limit or for very thin samples.

E. Optical Activity Terms

In the previous sections, an explicit derivation of the Mueller images has been presented. This derivation has been carried out in the first Born-Approximation, that is to say, in conditions in which the internal field is approximated by the incident field. This approximation somewhat limits the general validity of the formulae obtained, particularly their applicability to the prediction of optical activity effects.

The three main optical activity phenomena are: Optical Rotatory Dispersion (ORD), Circular Dichroism (CD), and CIDS. It has previously been shown (23) that objects in which the polarizability tensors associated with the scattering groups are not spherically symmetric, can show CIDS in scattering directions other than the forward direction. This is valid even if no coupling between polarizable groups is taken into account, as long as the groups are arranged in a chiral fashion. This is equivalent to saying that a first Born-Approximation suffices to describe this optical activity effect.

On the other hand, two different approaches can be used to introduce CD and ORD effects. The first approach consists of using the first Born-Approximation description and assuming that each polarizable group is intrinsically optically active, as presented in part III, section B. In this case, the optical activity arises only from the contributions of these chiral groups, but no optical activity can originate from the relative conformation of the groups in the object. This can be a reasonable way to treat these effects for not-too-optically dense systems. In these systems, the light does not depolarize substantially as it travels through the object and the optical activity effects dominate the terms M_{14} and M_{41} . In this case, these images contain the CD and ORD contributions at every position in the object. In particular, this approximation is quite good when a given domain in the object is made up of a large number of chiral molecules, which are otherwise randomly oriented within this domain. These domains can be considered to be optically isotropic at least to within dimensions of the order of the wavelength of light. In optical imaging, these are the dimensions of the smallest resolvable domain or pixel and, thus, the object can be considered locally isotropic. It should be kept in mind that, as mentioned earlier, the

sequential extinction process described by the Lambert-Beer law is itself a higher Born-Approximation effect and, thus, the first Born-Approximation is not strictly adequate. If much molecular orientation is present, on the other hand, the crystallinity will substantially depolarize the light and the correct description of the optical activity effects will depend strongly on the validity of the first Born-Approximation in treating the material under study.

The other method consists of introducing coupling between the polarizable groups and, thus, requires the use of higher Born-Approximations (23, 24). This is also necessary for the case of forward CIDS (23). The equations presented here can be easily modified and extended to higher Born-Approximations by realizing that the coupling between polarizable groups in a given molecule is equivalent to defining a new effective polarizability, as has been pointed out before (23). To extend the validity of the equations derived here to the second Born-Approximation, the polarizability α_i must be replaced by the new effective polarizability according to

$$\alpha_i^{\text{eff}} = \alpha_i^{\gamma\beta} \alpha_\gamma \alpha_\beta - \alpha_i^{\gamma\delta} \alpha_j^{\delta\eta} V_{ij}^{\beta\delta} a_\gamma a_\eta e^{i\mathbf{k}_0 \cdot \mathbf{r}_{ij}}, \quad (33)$$

where $\alpha_i^{\gamma\beta}$ and $\alpha_j^{\delta\eta}$ are the $\gamma\beta$ and $\delta\eta$ components of the polarizability tensors associated with groups i and j , respectively. \mathbf{r}_{ij} is the distance vector between these groups, and $V_{ij}^{\beta\delta}$ is given by

$$V_{ij}^{\beta\delta} = -4\pi k^2 \alpha_\beta \cdot \Gamma_{ij} \cdot \alpha_\delta.$$

Here Γ_{ij} is the coupling or interaction tensor between groups i and j . Notice that Eq. 33 above is not a true polarizability since its magnitude depends, in general, on the direction of propagation of the fields in the medium (\mathbf{k}_0), it nevertheless plays a role similar to that of a true polarizability and can be thought of as one.

Since the terms M_{i4} and M_{4j} are sensitive to the optical activity of an oriented system, the above results can be summarized as in Tables II and III. Only in the first Born-Approximation, we can say with certainty that the M_{14} and M_{41} are related to the pure optical activity of the object. Clearly, this optical activity can arise only as the result of some intrinsic chirality at the molecular level which, in general, has dimensions much smaller than the

TABLE II
IN DARK-FIELD IMAGING: M_{i4} OR M_{4j}

Contributions in first Born-Approximation	Contribution in higher Born-Approximations
Angle-dependent CIDS if no intrinsic optical activity is present	Angle-dependent CIDS
Scattering-detected CD and ORD if intrinsic optical activity is present	Scattering-detected CD and ORD Linear differential scattering and linear dichroism due to coupling depolarization

TABLE III
IN BRIGHT-FIELD IMAGING: M_{14} OR M_{41}

Contributions in first Born-Approximation	Contribution in higher Born-Approximations
None, if no intrinsic optical activity is present	Forward CIDS ORD CD
Forward CIDS, ORD, and CD if intrinsic optical activity is present	Linear differential scattering and linear dichroism due to coupling depolarization

wavelength of the light. For example, the presence of asymmetric carbons in hydrocarbons or the excitonic optical activity in nucleic acids. This approximation is supposed to be reasonable if the object is (a) not-too-optically dense and, (b) not-too-crystalline within dimensions of the order of light.

It should be mentioned, to conclude this section, that the form birefringence effects cannot be treated in the first Born-Approximation. These effects only arise out of higher Born-Approximations. In the first Born-Approximation, the only effects that can be included are those corresponding to intrinsic birefringence not arising from coupling mechanism.

IV. CONCLUSIONS

In the previous sections, we have presented a theory of differential polarization imaging following the Mueller matrix formalism. The equations predicting the sign and magnitude distribution of the intensities in the image plane, for each of the sixteen Mueller images, have been derived. This derivation has been carried out for both the dark-field and the bright-field imaging geometries and their main properties will be listed here.

(a) The first element (M_{11}) of the first column describes the regular unpolarized absorption and scattering, and the rest of the elements in the first column (M_{1i} [$i = 2, 3, 4$]) describe the regular absorption of unpolarized light and scattering affected by the appropriate analyzers. It can be shown that these terms in bright-field are related to the linear dichroism of the object (see paper II of this series). The second row requires the use of the horizontal and the vertical analyzers while the obliquely linear analyzers ($+45^\circ$ and -45° with reference to the horizontal axis) and the right- and left-circular analyzers must be used to obtain the Mueller images of the third and the fourth rows, respectively.

The first element of the second column is related to the linear differential scattering and the linear dichroism. The rest (M_{12} [$i = 2, 4$]) are related to the same phenomena if the sample is linearly anisotropic and not optically active (see paper II of this series). The first elements of the third and the fourth columns (M_{13} and M_{14}) are proportional to the oblique linear differential scattering and the oblique

linear dichroism, and the circular differential scattering and the circular dichroism, respectively. The rest of the elements in the third and the fourth column are discussed in paper II of this series, for the case of bright-field imaging.

(b) The dominant contribution to dark-field imaging is the differential scattering of polarized radiation due to the optical anisotropy of the object being imaged. The dark-field images are especially sensitive to structure with dimensions on the order of the wavelength of the incident light. Since the solid angle of light scattered by the object is relatively small and defined by the lens aperture, it is found that the spatial details of the dark-field images depend on scattering angles.

(c) In bright field Mueller imaging, there are generally three contributions: the incident light, the differential extinction (absorption and scattering), and the differential forward scattering. The term describing the incident light contributes only to the Mueller images in the diagonal of the Mueller matrix, i.e., in M_{ii} [$i = 1, 2, 3, 4$] and is virtually constant over the image. This term subtracts out and does not contribute to the off-diagonal Mueller images (M_{ij} , $i \neq j$).

The Mueller images M_{i4} and M_{4j} ($i, j = 1, 2, 3$) for a non-optically active medium have no contribution from forward differential scattering in the first Born-Approximation and when the incident wavelength falls outside the absorption bands of the object. In the first Born-Approximation, the secondary wavelets scattered by the groups in the object are all in phase and cannot interfere to yield a forward differential scattering contribution to M_{i4} and M_{4j} . Any mechanism that introduces a phase-shift between the wavelets scattered by the groups such as group-group interaction (20) (higher Born-Approximations) or energy dissipation (complex polarizabilities) will give rise to forward differential scattering. In particular, when absorption is allowed, the equations show that the wavelets arising from the real (diffractive) part of the polarizability of one group are 90° out-of-phase with the wavelets resulting from the imaginary (dissipative) part of the polarizability of another group. These wavelets can therefore interfere even in the forward direction, contributing to the Mueller images of the fourth row and column only if the individual groups are different from each other.

(d) The forward differential scattering contributes to the bright-field Mueller images M_{ij} ($i, j = 1, 2, 3$), even when the wavelength of the incident light falls outside the absorption bands and when the fields are obtained in the first Born-Approximation. The reason for this is that the contribution from forward differential scattering to these images only depends on the orientation of the polarizable axes of the groups, relative to the incident linear polarization. Thus, for linear polarizations, the forward differential scattering contribution does not require the interference of the wavelets as in the case of circular polarizations.

(e) In bright-field imaging when the incident wave-

length falls within an absorption band, the differential absorption mechanism dominates and forward differential scattering is negligible.

(f) $M_{ii} = 1$ ($i = 1, 2, 3, 4$) in bright-field imaging when there is no object.

APPENDIX A

To arrive at the right-hand side of Eq. 15, let us set the vector $k/r_0 \mathbf{r}_i + k\hat{\mathbf{r}}$ in the exponent of the left-hand side equal to \mathbf{q}_i whose basis vectors are $\hat{\mathbf{x}}$, $\hat{\mathbf{y}}$, and $\hat{\mathbf{z}}$. The direction of coordinates is chosen such that \mathbf{r}' is in the xy -plane. Then the scalar product $(r_0/k\mathbf{r}_i + k\hat{\mathbf{r}}) \cdot \mathbf{r}' = \mathbf{q}_i \cdot \mathbf{r}'$ becomes $q_i r' \sin \beta_i \cos(\phi' - \phi_i)$, where q_i is the magnitude of the vector \mathbf{q}_i , β_i is the angle between z -axis and \mathbf{q}_i , ϕ_i is the angle between x -axis and the projection of \mathbf{q}_i onto the xy -plane. If we replace da' with $r'dr'd\phi'$, we have the vectors \mathbf{q}_i and \mathbf{r}' in the spherical coordinate system. For a circular aperture of the radius a , the left-hand side of Eq. 15 becomes

$$\int_0^{2\pi} \int_0^\pi \exp[-iq_i r' \sin \beta_i \cos(\phi' - \phi_i)] r' dr' d\phi'. \quad (\text{A.1})$$

The integration of Eq. A.1 with respect to ϕ' can be performed using

$$\frac{1}{2\pi} \int_{-\pi}^\pi e^{iz \cos t} e^{im(t-\pi/2)} dt = J_m(z), \quad (\text{A.2})$$

where $J_m(z)$ is the cylindrical Bessel function of order m .

If we rearrange Eq. A.1 to make a similar form as Eq. A.2, we obtain

$$\int_0^a 2\pi r' \left[\frac{1}{2\pi} \int_0^{2\pi} e^{j(q_i r' \sin \beta_i) \cos(\phi' - \phi_i)} e^0 d\phi' \right] dr'. \quad (\text{A.3})$$

Changing the limits of the integration with respect to ϕ' , Eq. A.3 becomes

$$\begin{aligned} \int_0^a 2\pi r' \left[\frac{1}{2\pi} \int_{-\pi}^\pi e^{j(q_i r' \sin \beta_i) \cos(\phi' - \phi_i)} e^0 d\phi' \right] dr' \\ = 2\pi \int_0^a J_0(q_i r' \sin \beta_i) r' dr' \\ = 2\pi a^2 \frac{J_1(q_i a \sin \beta_i)}{q_i a \sin \beta_i}. \end{aligned} \quad (\text{A.4})$$

It can be seen that $q_i \sin \beta_i$ is the projection of the vector \mathbf{q}_i onto the xy -plane. Therefore,

$$\begin{aligned} q_i \sin \beta_i &= k \left[\left(\frac{x + x_i}{r + r_0} \right)^2 + \left(\frac{y + y_i}{r + r_0} \right)^2 \right]^{1/2} \\ &= \frac{k}{r} \left[\left(x + \frac{r}{r_0} x_i \right)^2 + \left(y + \frac{r}{r_0} y_i \right)^2 \right]^{1/2}, \end{aligned} \quad (\text{A.5})$$

where x and y are the Cartesian components of \mathbf{r} , and x_i and y_i are the x and y components of \mathbf{r}_i . Eq. A.5 is written in the following way when we notice that r/r_0 is the magnification, m , of the lens.

$$q_i \sin \beta_i = \left(\frac{k\rho_i}{r} \right), \quad (\text{A.6})$$

where

$$\rho_i = [(x + mx_i)^2 + (y + my_i)^2]^{1/2}.$$

Substituting Eq. A.6 into Eq. A.4, we obtain

$$2\pi a^2 \frac{J_1\left(\frac{k\rho_i}{r}\right)}{\frac{k\rho_i}{r}},$$

which is the right-hand side of Eq. 15.

APPENDIX B

To show that

$$\hat{\mathbf{f}} \times [\hat{\mathbf{z}} \times (\mathbf{I} - \hat{\mathbf{x}}_0 \hat{\mathbf{x}}_0) \cdot \mathbf{F} \cdot \hat{\mathbf{e}}_0] = (\hat{\mathbf{z}}\hat{\mathbf{f}} - \hat{\mathbf{f}} \cdot \hat{\mathbf{z}}) \cdot \mathbf{F} \cdot \hat{\mathbf{e}}_0,$$

notice first that $\hat{\mathbf{x}}_0 = -\hat{\mathbf{z}}$. Then

$$\begin{aligned} \hat{\mathbf{f}} \times [\hat{\mathbf{z}} \times (\mathbf{I} - \hat{\mathbf{x}}_0 \hat{\mathbf{x}}_0) \cdot \mathbf{F} \cdot \hat{\mathbf{e}}_0] &= \hat{\mathbf{f}} \times [\hat{\mathbf{z}} \times (\mathbf{I} - \hat{\mathbf{z}}\hat{\mathbf{z}}) \cdot \mathbf{F} \cdot \hat{\mathbf{e}}_0] \\ &= \hat{\mathbf{f}} \times [\hat{\mathbf{z}} \times (\mathbf{F} \cdot \hat{\mathbf{e}}_0)]. \end{aligned} \quad (\text{B.1})$$

The i th component is

$$\{\hat{\mathbf{f}} \times [\hat{\mathbf{z}} \times (\mathbf{F} \cdot \hat{\mathbf{e}}_0)]\}_i = \epsilon_{ijk} r_j [\hat{\mathbf{z}} \times (\mathbf{F} \cdot \hat{\mathbf{e}}_0)]_k.$$

This equation can be rewritten as

$$\epsilon_{ijk} r_j [\hat{\mathbf{z}} \times (\mathbf{F} \cdot \hat{\mathbf{e}}_0)]_k = \epsilon_{ijk} \epsilon_{lmk} r_j z_l (\mathbf{F} \cdot \hat{\mathbf{e}}_0)_m. \quad (\text{B.2})$$

Using the identity

$$\epsilon_{ijk} \epsilon_{lmk} = \delta_{il} \delta_{jm} - \delta_{im} \delta_{jl},$$

Eq. B.2 becomes

$$\begin{aligned} \epsilon_{ijk} \epsilon_{lmk} r_j z_l (\mathbf{F} \cdot \hat{\mathbf{e}}_0)_m &= \hat{\mathbf{z}}(\hat{\mathbf{f}} \cdot \mathbf{F} \cdot \hat{\mathbf{e}}_0) - (\hat{\mathbf{f}} \cdot \hat{\mathbf{z}})(\mathbf{F} \cdot \hat{\mathbf{e}}_0) \\ &= (\hat{\mathbf{z}}\hat{\mathbf{f}} - \hat{\mathbf{f}} \cdot \hat{\mathbf{z}}) \cdot \mathbf{F} \cdot \hat{\mathbf{e}}_0. \end{aligned}$$

APPENDIX C

The integration of Eq. 27 is done by assuming that the aperture of the lens is square and infinitely wide. Then, from Eq. 27,

$$\begin{aligned} \int_{\text{aperture}} e^{ik/2(1/r-1/f)(r')^2 - i\Delta\mathbf{k} \cdot \mathbf{r}'} da' \\ = \int_{-\infty}^{\infty} \int_{-\infty}^{\infty} e^{-ik/2r_0[(x')^2 + (y')^2]} e^{-i(\Delta k_x x' + \Delta k_y y')} dx' dy', \end{aligned} \quad (\text{C.1})$$

where x' and y' are the Cartesian components of \mathbf{r}' , and Δk_x and Δk_y are the x and y components of $\Delta\mathbf{k}$, and the thin lens formula, $1/r - 1/f = 1/r_0$ has been used. The integration of Eq. C.1 can be done using the result

$$\int_{-\infty}^{\infty} e^{-A^2 y^2} dy = \frac{\sqrt{\pi}}{A}$$

so that we obtain

$$\int_{\text{aperture}} e^{ik/2(1/r-1/f)(r')^2 - i\Delta\mathbf{k} \cdot \mathbf{r}'} da' = \frac{-i2\pi r_0}{k} \cdot e^{i(r_0/2k)(\Delta k_x^2 + \Delta k_y^2)}. \quad (\text{C.2})$$

Since

$$\Delta\mathbf{k} = \mathbf{k} - \mathbf{k}_0 = k \left(\frac{\mathbf{r}}{r} + \frac{\mathbf{x}_0}{r_0} \right)$$

then

$$\Delta k_x = \frac{kx}{r} \quad \text{and} \quad \Delta k_y = \frac{ky}{r}, \quad (\text{C.3})$$

where x and y are the Cartesian components of \mathbf{r} . Substitution of Eq. C.3 into Eq. C.2 yields Eq. 28.

APPENDIX D

To prove that the term proportional to the triadic $(\mathbf{I} \times \mathbf{F}^\dagger - \mathbf{F} \times \mathbf{I})_{\alpha\beta\gamma}$ in the bright-field equations of M_{i4} and M_{4j} ($i, j = 1, 2, 3, 4$) contains absorptive effects, we take M_{14} as an example. The term containing $(\mathbf{I} \times \mathbf{F}^\dagger - \mathbf{F} \times \mathbf{I})_{\alpha\beta\gamma}$ in the bright-field equation of M_{14} is

$$\frac{Ar_0^2}{a^2k^3} (\mathbf{I} \times \mathbf{F}^\dagger - \mathbf{F} \times \mathbf{I})_{\alpha\beta\gamma} \{(\hat{\mathbf{r}}\hat{\mathbf{z}} - \hat{\mathbf{r}} \cdot \hat{\mathbf{z}}) \cdot (\hat{\mathbf{z}}\hat{\mathbf{r}} - \hat{\mathbf{r}} \cdot \hat{\mathbf{z}})\}_{\alpha\gamma} \hat{\mathbf{k}}_{0\beta} \\ \propto \sum_i (\mathbf{I} \times \alpha_i^\dagger - \alpha_i \times \mathbf{I})_{\alpha\beta\gamma} (\mathbf{I} - \hat{\mathbf{k}}_0 \hat{\mathbf{k}}_0)_{\alpha\gamma} \hat{\mathbf{k}}_{0\beta}, \quad (\text{D.1})$$

where we have taken $\hat{\mathbf{r}} \approx \hat{\mathbf{z}} = \hat{\mathbf{k}}_0$. Now, we will show that the i th term in the right-hand side of Eq. D.1 is proportional to the circular dichroism of the i th group.

The power absorbed by a point polarizable group i is (11)

$$P_{\text{abs}} = \frac{ck|E_0|^2}{2} \text{Im}(\hat{\epsilon}_0 \cdot \alpha_i^* \cdot \hat{\epsilon}_0^*).$$

Since the absorbed power is proportional to the extinction coefficient ϵ , we have

$$\epsilon \propto \text{Im}(\hat{\epsilon}_0 \cdot \alpha_i^* \cdot \hat{\epsilon}_0^*).$$

Therefore, the circular dichroism of group i is

$$(\epsilon_L - \epsilon_R)_i \propto \text{Im}(\hat{\epsilon}_L \cdot \alpha_i^* \cdot \hat{\epsilon}_R) - \text{Im}(\hat{\epsilon}_R \cdot \alpha_i^* \cdot \hat{\epsilon}_L) \\ = (\hat{\epsilon}_L \cdot \alpha_i^* \cdot \hat{\epsilon}_R) - (\hat{\epsilon}_R \cdot \alpha_i \cdot \hat{\epsilon}_L) \\ - (\hat{\epsilon}_R \cdot \alpha_i^* \cdot \hat{\epsilon}_L) + (\hat{\epsilon}_L \cdot \alpha_i \cdot \hat{\epsilon}_R). \quad (\text{D.2})$$

Since $\hat{\epsilon}_L$ and $\hat{\epsilon}_R$ are orthogonal to $\hat{\mathbf{k}}_0$, Eq. D.2 can be written

$$(\epsilon_L - \epsilon_R)_i \propto (\hat{\epsilon}_L \cdot \mathbf{I}) \cdot (\mathbf{I} - \hat{\mathbf{k}}_0 \hat{\mathbf{k}}_0) \cdot (\alpha_i^* \cdot \hat{\epsilon}_R) \\ - (\hat{\epsilon}_R \cdot \mathbf{I}) \cdot (\mathbf{I} - \hat{\mathbf{k}}_0 \hat{\mathbf{k}}_0) \cdot (\alpha_i \cdot \hat{\epsilon}_L) \\ - (\hat{\epsilon}_R \cdot \mathbf{I}) \cdot (\mathbf{I} - \hat{\mathbf{k}}_0 \hat{\mathbf{k}}_0) \cdot (\alpha_i^* \cdot \hat{\epsilon}_L) \\ + (\hat{\epsilon}_L \cdot \mathbf{I}) \cdot (\mathbf{I} - \hat{\mathbf{k}}_0 \hat{\mathbf{k}}_0) \cdot (\alpha_i \cdot \hat{\epsilon}_R). \quad (\text{D.3})$$

Writing

$$\mathbf{I} - \hat{\mathbf{k}}_0 \hat{\mathbf{k}}_0 = \hat{\epsilon}_H \hat{\epsilon}_H + \hat{\epsilon}_V \hat{\epsilon}_V. \quad (\text{D.4})$$

Now substituting Eq. D4 into Eq. D.3, we obtain

$$(\epsilon_L - \epsilon_R)_i \propto [(\hat{\epsilon}_H \cdot \mathbf{I}) \cdot \hat{\epsilon}_L][\hat{\epsilon}_R \cdot (\alpha_i^\dagger \cdot \hat{\epsilon}_H)] \\ - [(\hat{\epsilon}_H \cdot \mathbf{I}) \cdot \hat{\epsilon}_R][\hat{\epsilon}_L \cdot (\alpha_i^\dagger \cdot \hat{\epsilon}_H)] \\ - [\hat{\epsilon}_R \cdot (\mathbf{I} \cdot \hat{\epsilon}_H)][(\hat{\epsilon}_H \cdot \alpha_i) \cdot \hat{\epsilon}_L] \\ + [\hat{\epsilon}_L \cdot (\mathbf{I} \cdot \hat{\epsilon}_H)][(\hat{\epsilon}_H \cdot \alpha_i) \cdot \hat{\epsilon}_R] \\ + [(\hat{\epsilon}_V \cdot \mathbf{I}) \cdot \hat{\epsilon}_L][\hat{\epsilon}_R \cdot (\alpha_i^\dagger \cdot \hat{\epsilon}_V)] \\ - [(\hat{\epsilon}_V \cdot \mathbf{I}) \cdot \hat{\epsilon}_R][\hat{\epsilon}_L \cdot (\alpha_i^\dagger \cdot \hat{\epsilon}_V)] \\ - [\hat{\epsilon}_R \cdot (\mathbf{I} \cdot \hat{\epsilon}_V)][(\hat{\epsilon}_V \cdot \alpha_i) \cdot \hat{\epsilon}_L] \\ + [\hat{\epsilon}_L \cdot (\mathbf{I} \cdot \hat{\epsilon}_V)][(\hat{\epsilon}_V \cdot \alpha_i) \cdot \hat{\epsilon}_R] \\ = i(\mathbf{I} \times \alpha_i^\dagger - \alpha_i \times \mathbf{I})_{\alpha\beta\gamma} (\mathbf{I} - \hat{\mathbf{k}}_0 \hat{\mathbf{k}}_0)_{\alpha\gamma} (\hat{\mathbf{k}}_0)_\beta,$$

where the vector identity

$$(\mathbf{c} \cdot \mathbf{a})(\mathbf{b} \cdot \mathbf{d}) - (\mathbf{d} \cdot \mathbf{a})(\mathbf{b} \cdot \mathbf{c}) \equiv (\mathbf{a} \times \mathbf{b}) \cdot (\mathbf{c} \times \mathbf{d})$$

has been used.

The authors thank Professor I. Tinoco, Jr. and Dr. M. F. Maestre for many helpful discussions.

This work was supported in part by grants from the National Institutes of Health GM-32543, National Science Foundation DMB-8609654 and DMB-8501024, a 1984 Searle's Scholarship, and an Alfred P. Sloan Fellowship. Additional support was obtained from the Center of High Technology and Materials, UNM. C. Bustamante is a 1984 Searle Scholar and a 1985 Alfred P. Sloan Fellow.

Received for publication 14 April 1987 and in final form 7 August 1987.

REFERENCES

- Mickols, W., I. Tinoco, Jr., J. E. Katz, M. F. Maestre, and C. Bustamante. 1985. Imaging differential polarization microscope with electron readout. *Rev. Sci. Instrum.* 56:2228-2236.
- Beach, D. A., K. S. Wells, F. Husher, and C. Bustamante. 1987. Differential polarization microscope using an image dissector camera and phase-lock detection. *Rev. Sci. Instrum.* In press.
- Mickols, W., C. Bustamante, M. F. Maestre, I. Tinoco, Jr., and S. H. Embury. 1985. Differential polarization microscopy: a new imaging technique. *Biotechnology.* 3:711-714.
- Mickols, W., M. F. Maestre, I. Tinoco, Jr., and S. Embury. 1985. Visualization of oriented hemoglobin in individual erythrocytes by differential extinction of polarized light. *Proc. Natl. Acad. Sci. USA.* 82:6527.
- Bustamante, C., M. F. Maestre, and K. S. Wells. 1986. Recent advances in polarization spectroscopy: perspectives of the extension to the soft x-ray region. *J. Photochem. Photobiol.* 44:331-341.
- Keller, D., C. Bustamante, M. F. Maestre, and I. Tinoco, Jr. 1985. Imaging of optically active biological structure by use of circularly polarized light. *Proc. Natl. Acad. Sci. USA.* 82:401-405.
- Shurcliff, W. A. 1962. *Polarized Light*. Harvard University Press, Cambridge, MA. 21.
- Van de Hulst, H. C. 1981. *Light Scattering by Small Particles*. Dover, New York. 42.
- Allen, F., and C. Bustamante. 1985. *Applications of Circularly Polarized Radiation Using Synchrotron and Ordinary Sources*. Plenum Publishing Corp., New York.
- Keller, D. 1984. Scattering optical activity of chiral molecules: circular intensity differential scattering and circular differential imaging. Ph.D. thesis. University of California, Berkeley.
- Jackson, J. D. 1976. *Classical Electrodynamics*. 2nd ed. John Wiley & Sons, Inc., New York. 441-442.
- Condon, E. U. 1937. Theories of optical rotary power. *Rev. Mod. Phys.* 9:432-457.
- Goodman, J. W. 1968. *Introduction to Fourier Optics*. McGraw-Hill Inc., New York. 77-80.
- Jenkins, F. A., and H. E. White. 1976. *Fundamentals of Optics*. 2nd ed. McGraw-Hill Inc., New York. 67.
- Born, M., and E. Wolf. *Principles of Optics*. 6th ed. Pergamon Press, Oxford.
- Bustamante, C., M. F. Maestre, and I. Tinoco, Jr. 1980. Circular intensity differential scattering of light by helical structure. I. Theory. *J. Chem. Phys.* 73:4273.
- Bustamante, C., I. Tinoco, Jr., and M. F. Maestre. 1982. Circular intensity differential scattering of light. IV. Randomly oriented species. *J. Chem. Phys.* 76:3440.
- Bustamante, C. 1980. Circular intensity differential scattering of chiral molecules. Ph.D. thesis. University of California, Berkeley.

19. Abhyankar, K. D., and A. L. Fymat. 1969. Relations between the elements of the phase matrix for scattering. *J. Math. Phys.* 10:1935–1938.
20. Bustamante, C., M. F. Maestre, D. Keller and I. Tinoco, Jr. 1984. Differential scattering (CIDS) of circularly polarized light by dense particles. *J. Chem. Phys.* 80:4817–4823.
21. Bohren, C. F., and D. R. Huffman. 1983. Absorption and Scattering of Light by Small Particles. John Wiley & Sons, Inc., New York.
22. Schellman, J. A., and H. P. Jensen. 1987. Polarization modulation spectroscopy. *Chem. Rev.* In press.
23. Keller, D., and C. Bustamante. 1968. Theory of the interaction of light with large inhomogeneous molecular aggregates. I. Absorption. *J. Chem. Phys.* 84:2972–2980.
24. Keller, D., and C. Bustamante. 1986. Theory of the interaction of light with large inhomogeneous molecular aggregates. II. Psi-type circular dichroism. *J. Chem. Phys.* 84:2961–2971.